



Meteorological controls on observed peroxyacetyl nitrate at Mount Bachelor during the spring of 2008

E. V. Fischer,¹ D. A. Jaffe,² D. R. Reidmiller,¹ and L. Jaeglé¹

Received 1 July 2009; revised 17 August 2009; accepted 19 October 2009; published 5 February 2010.

[1] A suite of gas phase and aerosol measurements were made during spring 2008 at the summit of Mount Bachelor (2763 m asl), located in central Oregon. Here we focus on observations of peroxyacetyl nitrate (PAN) for the period of 3 April to 18 June 2008. During this period, PAN mixing ratios ranged from below detection limit to 527 pptv, with a campaign mean of 119 pptv. Our analysis indicates that the variability in PAN was predominantly a function of synoptic scale processes. Three plumes containing elevated PAN were analyzed in detail. Two of these plumes were of Asian origin, and one was associated with North American sources. The Asian plumes were observed on 17–18 April and 12–13 May. Both were associated with elevated PAN, CO, O₃, and aerosol scattering (σ_{sp}). The relationship between PAN and O₃ varied with air mass temperature within the 17–18 April plume, and we exploited this to derive an O₃ production efficiency per unit of PAN decomposed of 51–73 mol mol⁻¹. The second Asian plume (12–13 May) was more dilute, characterized by lower CO and σ_{sp} . This event had a larger PAN/CO slope, consistent with relatively colder subsidence as calculated by trajectories. We traced the pathways of the plumes using a global chemical transport model (GEOS-Chem) alongside trajectories to show that the plumes crossed the Pacific at different rates and following different routes. The plume observed on April 17–18 traveled over the great circle, while the later plume took a slower more southern path across the Pacific.

Citation: Fischer, E. V., D. A. Jaffe, D. R. Reidmiller, and L. Jaeglé (2010), Meteorological controls on observed peroxyacetyl nitrate at Mount Bachelor during the spring of 2008, *J. Geophys. Res.*, 115, D03302, doi:10.1029/2009JD012776.

1. Introduction

[2] Asia is experiencing rapid economic growth and is a growing source of anthropogenic pollutants to the global atmosphere [Kato and Akimoto, 1992; van Aardeene *et al.*, 1999; Zhang *et al.*, 2007]. The demand for energy and an increased standard of living will result in increasing emissions of nitrogen oxides (NO_x = NO + NO₂) and nonmethane volatile organic compounds (NMVOC), both of which are ozone (O₃) precursors [Ohara *et al.*, 2007]. Emissions inventories indicate a ~176% increase in Asian NO_x emissions over the period 1980–2003, and both satellite measurements of the NO₂ column and emissions inventory approaches indicate an accelerating growth rate since 2000 [Ohara *et al.*, 2007; Richter *et al.*, 2005; Zhang *et al.*, 2007]. The increase in NO_x emissions over 1980–2003 was larger (~280%) in China, approximately 6% and 11% per year in the earlier and latter part of the period, respectively. Both emissions of NO_x and NMVOCs are projected to increase substantially through 2020 [Ohara *et al.*, 2007].

[3] Cyclones that develop over coastal East Asia provide the primary export pathway for pollutant plumes out of the Asian boundary layer (BL) [Bey *et al.*, 2001a]. Polluted BL air is drawn upward into the free troposphere (FT) between 30° and 60°N ahead of eastward moving cold fronts in warm conveyor belts [Liu *et al.*, 2003]. Only a fraction of the total reactive nitrogen (NO_y) emitted in the Asian BL is exported during this process. Koike *et al.* [2003] found that 15% of the NO_x emitted over northeastern China remained as NO_y over the western Pacific FT, and peroxyacetyl nitrate (PAN) was found to be the dominant form of NO_y [Koike *et al.*, 2003]. Observations of plumes over the Pacific Ocean during the Intercontinental Transport and Chemical Transformation (ITCT 2K2) experiment also indicated that most of the NO_y is not exported to the FT, primarily due to the loss of HNO₃ [Nowak *et al.*, 2004]. However, for PAN, frequent cyclone formation in spring, makes this an efficient season for export and eventual trans-Pacific pollution transport.

[4] The main loss process for PAN below ~7 km is via thermal decomposition (CH₃C(O)O₂NO₂ → CH₃C(O)O₂ + NO₂) [Talukdar *et al.*, 1995]. The lifetime of PAN is >1 month at temperatures characteristic of the midtroposphere in spring, but much shorter, on the order of 1 h, at 20°C. Because PAN has a relatively long lifetime at low temperatures, it can be transported on a hemispheric scale in the midtroposphere, thereby serving as a reservoir for reactive nitrogen. It can subsequently decompose under subsiding synoptic regimes to release NO_x in remote areas. Measurements

¹Department of Atmospheric Sciences, University of Washington, Seattle, Washington, USA.

²Science and Technology Program, University of Washington Bothell, Bothell, Washington, USA.

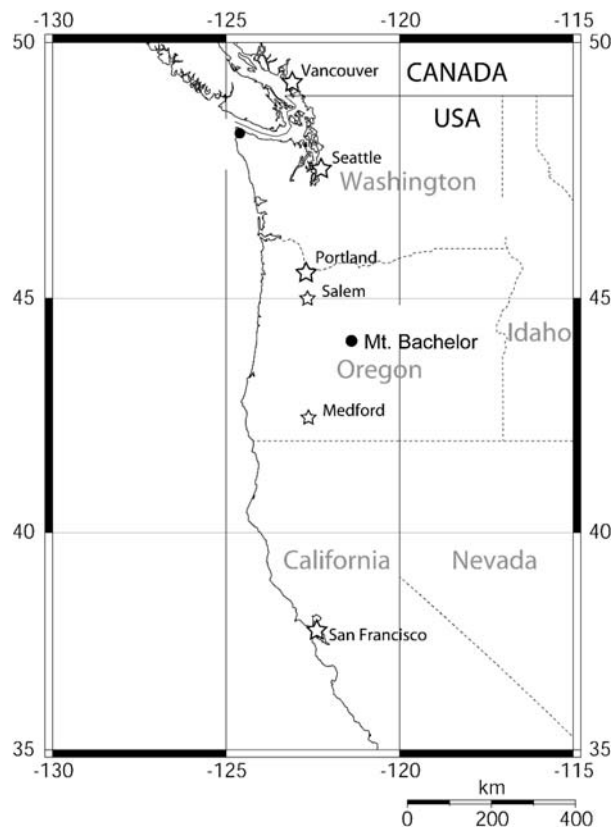


Figure 1. Location of Mount Bachelor and other relevant sites. Map adopted from Weiss-Penzias *et al.* [2006].

of PAN and NO_x in the remote troposphere support this view [Singh and Salas, 1986]. The cyclonic export mechanism from the Asian source region and the synoptic scale subsidence that delivers plumes from the FT to the surface create the episodic nature of Asian pollution impacting North America [Yienger *et al.*, 2000].

[5] The impact of Asian NO_x emissions on North American surface O_3 concentrations can be divided into direct transport of O_3 produced in the Asian BL and in-transit production from the export of NO_x and PAN [Jaeglé *et al.*, 2003]. Ozone has a relatively long photochemical lifetime during spring (~ 1 month), so O_3 exported from the Asian continent can have an impact on downwind regions [Heald *et al.*, 2003]. NO_x produced from the thermal decomposition of PAN has been suggested to enhance O_3 production in descending Asian pollution plumes observed in the eastern Pacific FT [Heald *et al.*, 2003; Hudman *et al.*, 2004; Kotchenruther *et al.*, 2001; Moxim *et al.*, 1996; Zhang *et al.*, 2008].

[6] Here we report on spring 2008 PAN observations from Mt. Bachelor (2763 m), a mountain top site located in central Oregon. We use the data to characterize the variability of PAN observed at Mt. Bachelor during spring 2008, and we use local meteorological parameters to separate measurements of PAN in the FT from BL-influenced periods. We present case studies of two major PAN events in the context of air mass origin using backward trajectories and the 3D global chemical transport model GEOS-Chem, and we compare these events to the climatological mean synoptic conditions associated with trans-Pacific O_3 transport [Zhang

et al., 2008]. Observations of O_3 and PAN during the largest PAN episode are used to estimate the contribution of thermal PAN decomposition to O_3 production, and we compare this estimate to the limited previous estimates.

2. Methods

2.1. Site Description

[7] Mount Bachelor Observatory (MBO) is located on the summit of a dormant volcano in central Oregon (43.98°N 121.7°W , 2763 m asl) (Figure 1). Since its establishment, MBO has proven to be well positioned to observe Asian air pollution and biomass burning plumes [Jaffe *et al.*, 2005; Weiss-Penzias *et al.*, 2007, 2006].

[8] The sampling inlet is located on the roof of the summit lift building, and the instruments are located in a temperature-controlled room within the building, situated approximately 15 m lower than the inlet. CO , O_3 , NO_x , and PAN were sampled through a $1/4''$ internal diameter PFA Teflon line, with a $1\ \mu\text{m}$ Teflon filter located at the inlet. All instruments were connected to the line through a common Teflon manifold, and flow through the line was $\sim 14\ \text{L}\ \text{min}^{-1}$ resulting in a residence time of $\sim 2\ \text{s}$. Midvisible (530 nm) sub- μm σ_{sp} was measured using a Radiance Research (M903) nephelometer. Temperature (T), relative humidity (RH), pressure (P), and wind direction were also measured at the summit. The methods pertaining to the ongoing measurements other than PAN have been described in detail previously [Weiss-Penzias *et al.*, 2006]. Multiwavelength measurements of sub- μm dry aerosol σ_{sp} and aerosol absorption (σ_{ap}) were also measured during spring 2008 using a three wavelength integrating nephelometer (Model TSI-3563, TSI Incorporated, Shoreview, MN) and a three wavelength Particle Soot Absorption Photometer (PSAP, Radiance Research, Seattle, WA). This aerosol data is reported at standard temperature and pressure (STP), and these particular measurements are described in a separate paper [Fischer *et al.*, 2009, manuscript in preparation]. NO was measured with a high-sensitivity chemiluminescence instrument similar to that described by Kotchenruther *et al.* [2001]. NO_2 was detected as NO following broadband UV photolysis using a Droplet Measurement Technology Blue Light Converter. The NO_x measurements are described in detail in a separate paper [Reidmiller *et al.*, 2009, manuscript in preparation]. Unless otherwise noted, all data are reported in GMT which is 7 h later than local Pacific Daylight Time (GMT = PDT + 7).

2.2. PAN Measurements

2.2.1. Instrument Design

[9] PAN was measured with a custom gas chromatograph with a Shimadzu Mini2 electron capture detector (ECD). A schematic diagram is provided in Figure 2. A 1.5 mL sample was injected using an eight-port Valco sampling valve. The sample loop is made from $1/8''$ polyetheretherketone (PEEK) tubing and the connecting tubing material from the sampling valve to the column is $1/16''$ PEEK. We chose PEEK tubing over perfluoroalkoxy (PFA) and stainless steel because oxygen diffuses through PFA tubing, causing an elevated and noisy background, and PAN loss has been observed on stainless steel. Flocke *et al.* [2005] reported no loss of PAN in PEEK tubing. Ultrahigh purity (UHP) helium (He) was used as a

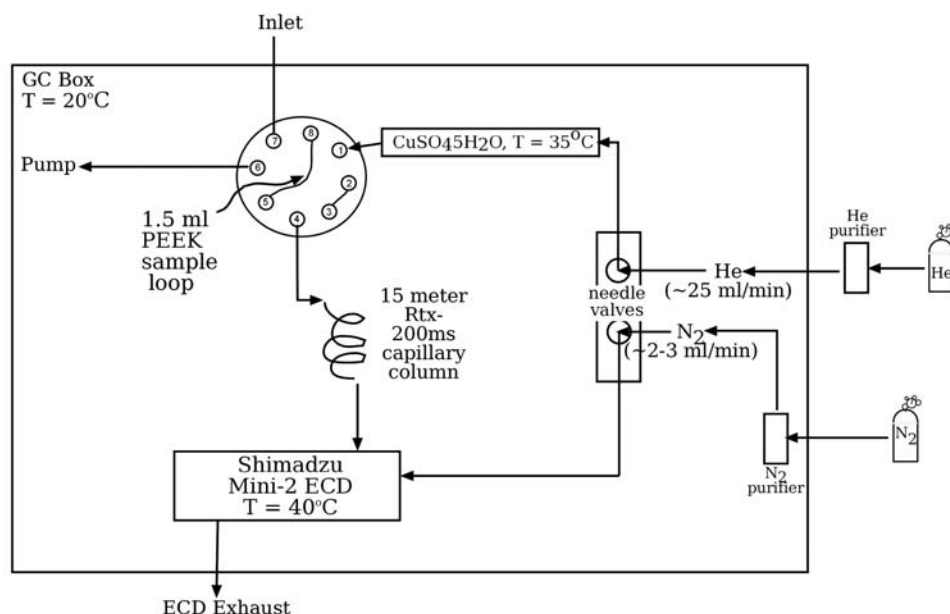


Figure 2. Schematic of the custom gas chromatograph.

carrier gas, and UHP nitrogen (N_2) was used as a make-up gas. The carrier gas was further purified with a Valco Helium Purifier (HP2) to remove a suite of impurities, most importantly O_2 . The UHP N_2 passed through an O_2 and H_2O trap (Supelpure-O 22449). The carrier gas flow rate was $\sim 25 \text{ mL min}^{-1}$, and the make-up gas flow was $2\text{--}3 \text{ mL min}^{-1}$.

[10] The air masses encountered at MBO have a similar range of water vapor (WV) mixing ratios to those sampled during aircraft campaigns. Following *Flocke et al.* [2005], prior to entering the valve and column the carrier gas was humidified with 100 ppmv WV. This was accomplished by passing the carrier gas through a cartridge filled with $\sim 200 \text{ g}$ of copper(II) sulfate pentahydrate ($CuSO_4 \cdot 5H_2O$, 99.995% purity), temperature controlled to 35°C [*Flocke et al.*, 2005]. Prior to installing the cartridge in the system, it was flushed with UHP He (at $\sim 50 \text{ mL min}^{-1}$) for several days. The addition of WV minimizes loss of PAN in the column, valve, and connecting tubing. The cartridge was changed monthly.

[11] We used a 15 m Restek Rtx-200 ms ($1 \mu\text{m}$ film thickness, 0.53 mm ID) capillary column to separate PAN. The carrier gas and makeup gas flows are controlled using two nonlubricated low-flow needle valves (Valco ZBNV1LF-D). The eight-port valve, connecting tubing, needle valves, and column are situated in an insulated box which is controlled to 20°C using a bidirectional temperature controller (TE Technology TC 36–25 RS232) and a thermoelectric device (TE Technology AC-073) with a built-in Peltier cooler element, and hot and cold side fans. This temperature and flow rate setting yields a PAN retention time of $\sim 1.9 \text{ min}$. By controlling the temperature of all the components, we are able to ensure a constant sample volume, retention time, and minimize baseline drifting. The room temperature was also controlled at $20 \pm 3^\circ\text{C}$. The PAN spends 2 min within the instrument. At 20°C , PAN has a lifetime for thermal dissociation of about 85 min, which yields a thermal loss of

about 3% during the sample time within the instrument; however, this is corrected through our calibration system.

[12] The Shimadzu Mini2 ECD was operated using a custom NOAA GMD electrometer. The detector was insulated and temperature was independently controlled to 40°C . The ECD was operated in constant-current mode ($144.0 \text{ picoamperes}$), which yielded a background voltage of approximately 150 mV. The output voltage signal from the electrometer was converted to a digital signal by the Peak Simple Chromatography Data System. Peak Simple software was used to collect the output from the electrometer at 5 Hz, and it was also used to perform the integrations. Sample chromatograms are given in Figure 3. Samples were injected every 10 min, and each sample is a point measurement, not a 10-min average. Both hourly averages and unaveraged data are used in our analysis. Each hourly average includes all samples taken within that hour, normally 6.

2.2.2. Calibration, Uncertainty, Sensitivity, and Detection Limit

[13] We used a photochemical PAN calibration source similar to that described by *Roberts et al.* [2004] and *Wolfe et al.* [2007]. Peroxyacetyl radicals were generated by the photolysis of acetone (20 ppm acetone in ultra zero air, Scott-Marrin) in the presence of O_2 . An accurately measured flow of NO was added to the acetone gas stream. In this system, the NO is converted to NO_2 and then to PAN [*Roberts et al.*, 2004; *Warneck and Zerbach*, 1992]. The output from the calibrator was diluted with hydrocarbon free air from a pressurized cylinder. We assumed that the calibrator was $93 \pm 3\%$ efficient in converting NO to PAN [*Volz-Thomas et al.*, 2002]. Calibrations were accomplished by switching the inlet line from the common manifold to the calibrator exhaust line. A small portion of the calibrator exhaust was pulled into the sample loop, and calibration samples were handled exactly the same as the ambient samples. One-point calibrations were done weekly throughout the campaign and

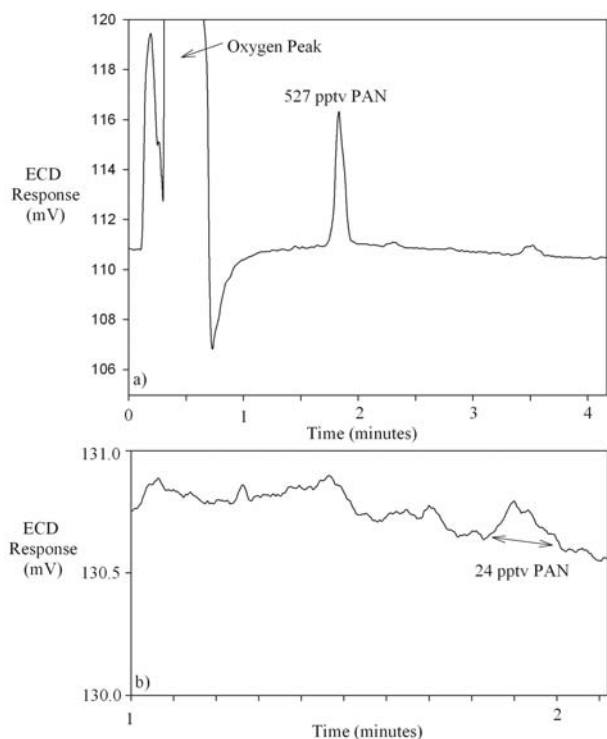


Figure 3. Examples of PAN chromatograms: (a) 18 April 2008 and (b) 18 May 2008. The signal in Figure 3a corresponds to an ambient mixing ratio of 527 pptv PAN, the maximum mixing ratio measured during the campaign. The large signal before 1 min is the oxygen peak. The signal in Figure 3b corresponds to an ambient PAN mixing ratio of 24 pptv.

were supplemented by multipoint calibrations every 2 weeks. We used an Airgas standard cylinder with a NO mixing ratio of 0.82 ± 0.01 ppm. This cylinder was compared to a 10.12 ppm National Institute of Standards and Technology (NIST)-traceable Scott-Marrin cylinder prior to and following the spring 2008 campaign to ensure that the mixing ratio in the Airgas cylinder did not drift during the campaign.

[14] We estimate the accuracy of the PAN mixing ratio produced by the calibrator to be 7.7%. This was calculated as the root sum of the squares of the error in all the calibration components, which includes the reported uncertainty in the mixing ratios of the calibration gases (5.0%), the uncertainty of the flow controllers used to deliver the calibration gases to the calibrator (1.7%, 0.89%, 0.29% for the three flow controllers) and the uncertainty associated with the calibrator efficiency (3.0%). On the basis of multiple calibrations, the estimated precision of the system is 3.0%. The overall uncertainty in each sample was 8.2% and this was calculated as the root sum of the squares of the precision (3.0%) and the accuracy (7.7%). On the basis of chromatograms taken during clean air periods, we estimate an on-site detection limit of ~ 15 pptv. This corresponds to a peak height-to-baseline noise ratio of 3.

[15] The average sensitivity throughout the campaign was 13.9 ± 0.7 (mean ± 1 SD) area units per pptv. The PAN mixing ratio in a given sample is found by multiplying the

area of the peak by the sensitivity. With the exception of one 2-week period, PAN mixing ratios were determined using the average sensitivity of the encompassing biweekly multipoint calibrations. During the one period where there was a change of more than 7% between subsequent biweekly calibrations, a linear fit between the two biweekly multipoint calibrations was used to determine the sensitivity and the corresponding PAN mixing ratios for this period.

2.3. Description of Backward Trajectories

[16] We calculated two sets of backward trajectories to establish the long-range transport history of the air masses impacting MBO. The first set included 10-day back trajectories initialized each hour from the summit of MBO using the Hybrid Single-Particle Lagrangian Integrated Trajectory (HYSPPLIT-4) model [Draxler and Rolph, 2003]. These 10-day trajectories were calculated using global meteorological data from the Global Data Assimilation System (GDAS) archive, which has a time resolution of 3 h, a spatial resolution of 1° latitude by 1° longitude, and a vertical resolution of 23 pressure surfaces between 1000 and 20 hPa. Trajectories were run at multiple heights surrounding the summit of MBO as described by Weiss-Penzias *et al.* [2006].

[17] The second set of backward HYSPLIT trajectories were run for 3 days using meteorological data from the Eta Data Assimilation System (EDAS) archive. The EDAS archive grid covers the continental United States after 2004, has a horizontal resolution of 40 km and a vertical resolution of 26 pressure surfaces between 1000 and 50 hPa. These trajectories were initialized from 1200 m above model ground level (amgl) for each hour of the spring campaign. The trajectories were initialized above the ground since both the GDAS and the EDAS models define the terrain for the grid box containing MBO significantly below the actual altitude of Mount Bachelor.

[18] Error in HYSPLIT trajectory calculations normal to the direction of flow are 10–30% of the distance traveled after 24 h [Draxler and Hess, 1998]. A trajectory is not representative of the path of an air parcel within the BL because the parcel quickly loses its identity through mixing processes [Stohl, 1998]. However, the HYSPLIT model is adequate to classify regional-scale air mass motions.

2.4. Temperature and Relative Humidity Profiles

[19] During spring 2008, we used a novel method to acquire in situ profiles of T and RH along the northwest face of Mount Bachelor. The goals of these measurements were to determine if the local BL reaches the summit and if so, at what time does this occur. We employed a HOBO (<http://www.onsetcomp.com/>) model S-THA-M002 T/RH sensor, Model # S-BPA-CM10 barometric pressure sensor and a model H21-002 Micro Station (to log the 1 s data). These components were sheltered in a custom-made PVC housing, specifically designed to allow ample airflow to pass over the sensors, ensuring sufficient response times. The ~ 0.5 m long instrument was attached to the back of a chair on the ski resort's chair lift that runs from midmountain (~ 2230 m asl) to the summit (~ 2700 m asl) where our trace gas species are measured. Using barometric pressure as a proxy for altitude, we were able to track the temporal evolution of changes to the mixed layer from early morning ($\sim 08:00$ PDT) until early afternoon ($\sim 13:00$ PDT). These observations were made on

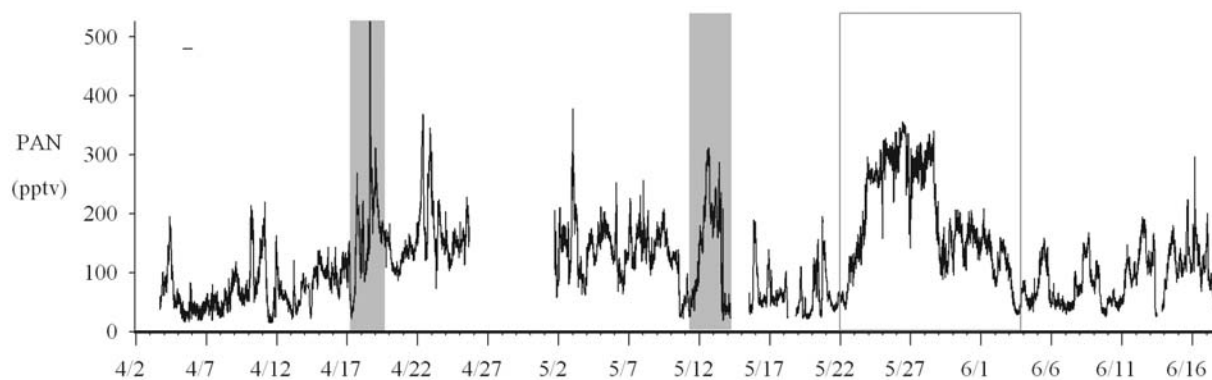


Figure 4. Time series of 10-min PAN for spring 2008. Data for March was intermittent and has not been included here. The shaded periods represent the two periods of strong Asian influence that are discussed in detail in section 3.2. The gray box encompasses the period of consistent North American continental influence, also discussed in section 3.5.

8 days over the campaign, and they provide information on BL evolution under a variety of meteorological conditions [Reidmiller *et al.*, manuscript in preparation]. The profiles are used in this analysis to overcome the challenges associated with interpreting measurements of pollution plumes impacting MBO in the context of local BL dynamics.

2.5. Model Description

[20] We used the GEOS-Chem global 3-D transport model of tropospheric chemistry version v8-01-03 (<http://www.as.harvard.edu:16080/chemistry/trop/geos/>) [Bey *et al.*, 2001b] to aid our interpretation of the MBO data. The model was driven by assimilated meteorological fields from the Goddard Earth Observing System (GEOS-5) of the NASA Global Modeling and Assimilation Office (GMAO). The GEOS-5 meteorological fields were degraded to a horizontal resolution of 2° latitude by 2.5° longitude. The GEOS-5 meteorology has a time resolution of 3 h for surface fields and 6 h for the rest of the atmosphere. We use a vertical resolution with 47 levels, with 15 levels below 2 km.

[21] We used the 2008 Fire Locating and Modeling of Burning Emissions (FLAMBE) daily biomass burning emissions [Reid *et al.*, 2004] and 2001 Asian emissions [Streets *et al.*, 2006]. North American anthropogenic emissions are based on the Environmental Protection Agency National Emission Inventory (EPA-NEI99) for the United States, the Criteria Air Contaminants (CAC) inventory for CANADA, and the Big Bend Regional Aerosol and Visibility Observational Study Emissions Inventory (BRAVO) [Kuhns *et al.*, 2005] for Mexico. European anthropogenic emissions are from the Cooperative Programme for Monitoring and Evaluation of the Long-range Transmission of Air Pollutants in Europe (EMEP) inventory [Vestreng and Klein, 2002]. Anthropogenic emissions elsewhere are based on the EDGAR 2000 inventory [Olivier *et al.*, 1999]. Biogenic emissions are from the Model of Emissions of Gases and Aerosols from Nature (MEGAN) inventory [Guenther *et al.*, 2006].

[22] We conducted a full chemistry O_3 - NO_x -VOC-aerosol simulation to examine the distribution of PAN. In addition, we also conducted a CO-only simulation in which CO tracers were tagged according to their source regions and type. In

particular, we will present results of a tagged CO tracer for biomass burning occurring in Siberia, defined as the Asian region poleward of $33^\circ N$ and eastward of $60^\circ E$.

3. Results and Discussion

3.1. Overview of Chemical Measurements

[23] Figure 4 presents a time series of the 10-min PAN data for the spring 2008 campaign. PAN mixing ratios were relatively low during the first half of April (median = 62 pptv). The gray shading highlights two periods of elevated PAN where backward trajectories indicate that the air masses likely spent significant time in the Asian BL prior to reaching MBO. The first of these events occurred in mid-April and the maximum single point observation of PAN during the campaign (527 pptv) occurred during this period. The second event occurred in mid-May; both events are discussed in detail in section 3.2. The gray box surrounds an obvious weeklong period of elevated PAN and this was a period of North American continental influence. This event is discussed in section 3.5.

[24] Table 1 presents an overview of the hourly averaged data (mean $\pm 1\sigma$) during April and May 2008. The mean PAN mixing ratio (119 pptv) for the campaign was larger than the median (109 pptv) reflecting sporadic elevated events. Higher mean O_3 and CO were observed during April than May reflecting the expected seasonality of these species at a remote site [Derwent *et al.*, 1998; Holloway *et al.*, 2000; Logan, 1985].

[25] To facilitate a more direct comparison of the 2008 MBO PAN data with aircraft data from previous campaigns in the eastern Pacific region, the hourly averaged data were segregated on the basis of the associated average WV mixing ratio. The WV bounds chosen for each month created two data sets with different characteristics. The “wet” data set is representative of BL influenced air. The “dry” data set is representative of pure FT air, or air that is characteristic of 700 hPa (~ 3 km) and higher. Fifteen day running statistics were calculated using the WV mixing ratio reported at 850 and 700 hPa for the routine Medford and Salem, OR (Figure 1) atmospheric soundings (<http://weather.uwyo.edu/upperair/sounding.html>). The MBO data were classified as “wet” if

Table 1. Hourly Mean ($\pm 1\sigma$) Monthly Values for the Chemical and Meteorological Parameters Measured During April and May 2008^a

Month and Segregation, N	PAN, pptv	CO, ppbv	O ₃ , ppbv	NO, pptv	NO ₂ , pptv	σ_{sp} , Mm ⁻¹	T, °C	Relative Humidity, %	Water Vapor, g/kg
April dry data (149)	147 ± 48	147 ± 9	55 ± 5.6	10 ± 12	104 ± 54	4.5 ± 7.4	-12 ± 3.5	82 ± 17	1.7 ± 0.3
April wet data (491)	88 ± 58	135 ± 20	52 ± 6.9	25 ± 34	112 ± 77	4.1 ± 4.8	-4.3 ± 5.5	84 ± 16	3.17 ± 0.9
April all data (533)	109 ± 63	138 ± 19	53 ± 6.6	20 ± 29	110 ± 69	4.0 ± 5.2	-6.4 ± 5.9	84 ± 16	2.0 ± 0.7
May dry data (44)	140 ± 50	142 ± 17	63 ± 6.7	7.5 ± 7.4	85 ± 64	2.5 ± 4.6	-5.1 ± 4.1	52 ± 27	1.7 ± 0.5
May wet data (650)	129 ± 90	125 ± 21	46 ± 10	26 ± 39	101 ± 59	3.3 ± 3.8	1.1 ± 5.2	82 ± 19	4.6 ± 1.1
May all data (724)	130 ± 87	127 ± 22	48 ± 11	23 ± 37	100 ± 59	3.1 ± 3.8	0.4 ± 5.5	79 ± 21	3.1 ± 1.0

^aSee section 3.1 for an explanation of the “wet”(representative of 850 hPa) and “dry” (representative of 700 hPa) classifications.

the WV mixing ratio were greater than the 25th percentile of the Medford and Salem sounding data at 850 hPa for the surrounding 15 days. Similarly, the MBO data were classified as “dry” if the WV mixing ratio was less than the 75th percentile of the sounding data at 700 hPa for the surrounding 15 days.

[26] Table 1 presents the mean $\pm 1\sigma$ for the relevant chemical and meteorological parameters in both the “wet” and “dry” data subsets. The difference between the average O₃ in the two data sets was modest in April and larger in May when we expect more thermally driven BL influence. PAN and CO mixing ratios and σ_{sp} were larger in the “dry” data than in the “wet” data, with a larger difference in April. This reflects enhanced global sources of these compounds to the FT and relatively few local sources in this region.

[27] To determine the degree to which daily upslope and downslope mountain flows influenced the measured chemical species, we calculated the average value of each parameter as a function of time of day. The range of variability in the PAN diurnal cycle was an order of magnitude smaller than the range of PAN measurements, suggesting that diurnal processes are not a main factor controlling PAN levels at MBO. The average PAN mixing ratio (127 pptv) during the afternoon hours was slightly higher than the average PAN mixing ratio during the morning hours (116 pptv), but the *z*-statistic indicated that the difference was not significant. There was a notable afternoon/early evening rise in PAN observed on several days during May, and this was possibly attributable to thermally induced vertical transport of BL pollution [Zellweger *et al.*, 2003]. Averaged over April and May, the hourly average NO_x mixing ratio reached a minimum at 8:00 PDT (94 pptv) and a maximum at 19:00 PDT (180 pptv). The hourly average afternoon NO peak (50 pptv) occurred at 15:00 PDT. The diurnal cycles of the routine measurements (O₃ and CO) have been summarized previously by Weiss-Penzias *et al.* [2006] and will not be repeated here.

3.2. Analysis of the Asian Pollution Transport Events

3.2.1. The 17–18 April Plume

[28] In this section, we focus our attention on the largest PAN plume observed during the spring 2008 campaign. The plume was observed over a 24 h period, and we use the in situ chairlift profiles of *T* and RH to identify predominantly FT-influenced periods. We begin with a description of the gas and aerosol observations, followed with a discussion of the meteorological context. Finally, we break the event into two periods on the basis of subsidence temperature and calculate the O₃ production likely resulting from PAN decomposition.

[29] Elevated σ_{sp} , CO, O₃, and PAN mixing ratios were observed from 17 April 1300 GMT to 18 April 1900 GMT;

a time series of these parameters is presented in Figure 5a. The peak PAN mixing ratio during spring 2008 was observed toward the end of this period on 18 April 1500 GMT. At times when the PAN peaked, a simultaneous spike in O₃ was also observed. CO reached 195 ppbv coincident with the PAN peak; however, CO measurements were only available after 17 April 2100 GMT. During the period with both CO and PAN measurements, CO and PAN were well correlated ($R^2 = 0.66$). The relationship between O₃ and PAN differed during the two morning periods. There was a larger O₃ enhancement during the morning of 17 April and a smaller O₃ enhancement relative to the PAN enhancement on the morning of 18 April. The maximum hourly average NO₂ mixing ratio (523 pptv) measured during the campaign also occurred during the afternoon of 18 April. The NO₂ peak of 184 pptv observed at 1300 GMT 18 April stands apart from the average NO₂ mixing ratios for this time of day, which were typically <100 pptv.

[30] Figures 6a and 6b present representative 10 day HYSPLIT back trajectories for the event. The trajectories shown in Figure 6 represent the 5 h period surrounding the peak measured PAN mixing ratio. Trans-Pacific transport was relatively efficient; the plume crossed along the Pacific Rim in approximately 5 days. Figures 6c and 6d are summaries of all the 10-day back trajectories for the time period of interest. The *y* axis in each plot is the height that the trajectories were initialized at MBO, and the color indicates how many hours a particular trajectory, initialized at a given height and time, spent within the two boxes shown in Figure 6a.

[31] The northern box in Figure 6a encompasses a region where there were many active forest fires during mid-April 2008. Active fires for 12–14 April, as identified by MODIS, are plotted in red for this region (<http://maps.geog.umd.edu/firms/>) [Davies *et al.*, 2009; Giglio and Descloitres, 2003; Justice *et al.*, 2002]. The trajectories show that the air mass impacting MBO on 17–18 April passed through this area of active forest fires in southeastern Russia between 12 April and 14 April. Some of the trajectories also passed through a region of intense agricultural burning further west (not shown). Biomass burning emissions can be a source of PAN, as the emissions are relatively high in both NO_x and acetaldehyde [Trentmann and Andreae, 2003]. Without tracer measurements (e.g., CH₃CN) and given the large error in trajectory calculations, we are unable to determine whether this plume has a primarily fossil fuel or biomass-burning source using the observations alone. However, the GEOS-Chem tagged CO simulation does support a Siberian biomass-burning source. After the plume was exported from the Asian BL, it was primarily transported above 4 km.

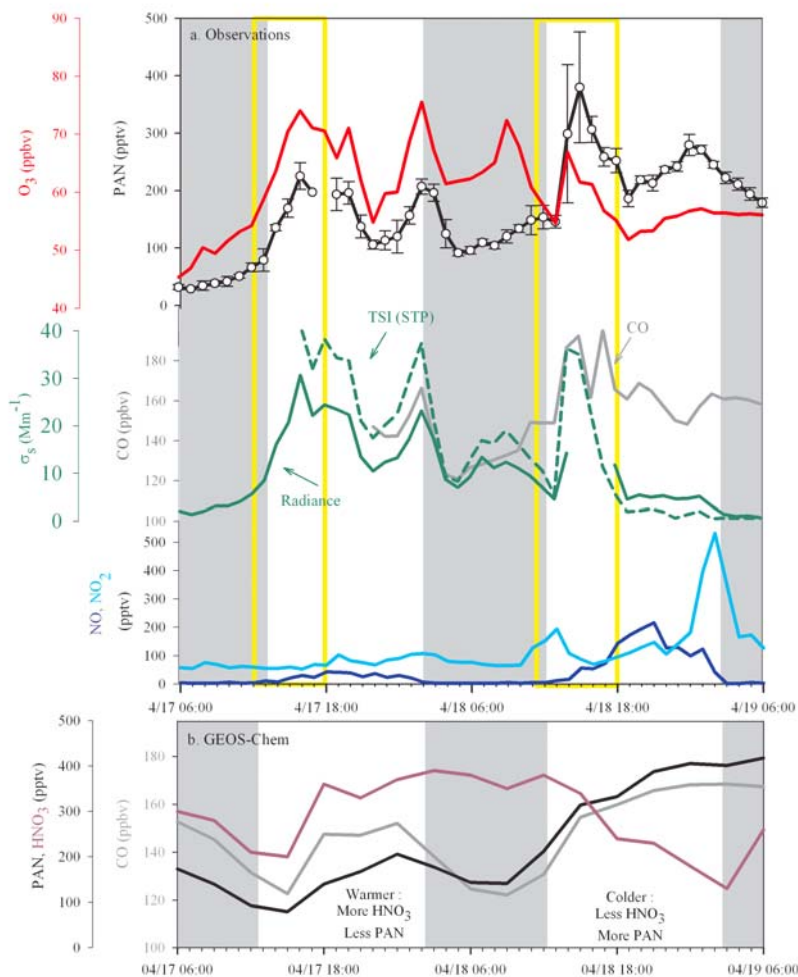


Figure 5. (a) Time series of gas and aerosol species on 17–18 April. PAN error bars are $\pm 1\sigma$ of the measurements included in each hourly average. All the other data are presented as hourly averages. Two measures of σ_{sp} are included here because of breaks in the data. The TSI data have been corrected to STP, the radiance data have not. The shading indicates approximate sunset to sunrise and time is in GMT. The yellow boxes surround the two FT-influenced morning periods used in the calculations presented later in Table 2. (b) GEOS-Chem simulated CO, HNO_3 , and PAN for the location of MBO.

The trajectories suggest that the plume began to descend south of Alaska.

[32] The air mass arrived at MBO under strongly subsiding conditions. The WV mixing ratio coincident with the peak PAN was 1.9 g/kg, and reached a minimum of 1.6 g/kg a few hours earlier. Figure 7a shows the dropping temperature and pressure (solid lines) observed at MBO throughout the event. Figure 7 also shows the initialization pressure and temperature from the EDAS 40 km trajectories (dashed lines). These parameters track the observations, indicating that the trajectories and the underlying meteorological fields captured the regional synoptic situation well. The plume subsided during a period of cold air advection over the Pacific Northwest.

[33] The lower panel of Figure 7a shows the RH and WV observed at MBO. On the basis of average WV mixing ratios for routine nearby Medford, OR (Figure 1) soundings, the air reaching MBO during the peak PAN was characteristic of ~ 700 hPa. It should be noted that this is approximate since WV mixing ratios at a given altitude vary widely. The

observed minima in σ_{sp} near sunrise on 18 April (Figure 5a) coincides with a period of high RH, suggesting that the aerosols may have been scavenged locally.

[34] Figure 7b shows the evolution of the local specific humidity (q) profile during the morning period of 18 April. These are in situ profiles of q for two time periods (0845 and 1145 PDT) on 18 April. These profiles extend from approximately midmountain to the summit where the other observations are made, and they can be used to infer the evolution of the local BL. The times given are approximate since each vertical profile was taken over a period of approximately 12 min. In situ profiles were not collected on 17 April.

[35] The in situ soundings show that during the morning, notably during the time of the peak observed PAN mixing ratio (~ 0800 PDT), the summit was not impacted by the BL, where q is expected to be constant with height. Throughout the morning, the height of the BL increased, reaching the summit around midday. The in situ profiles

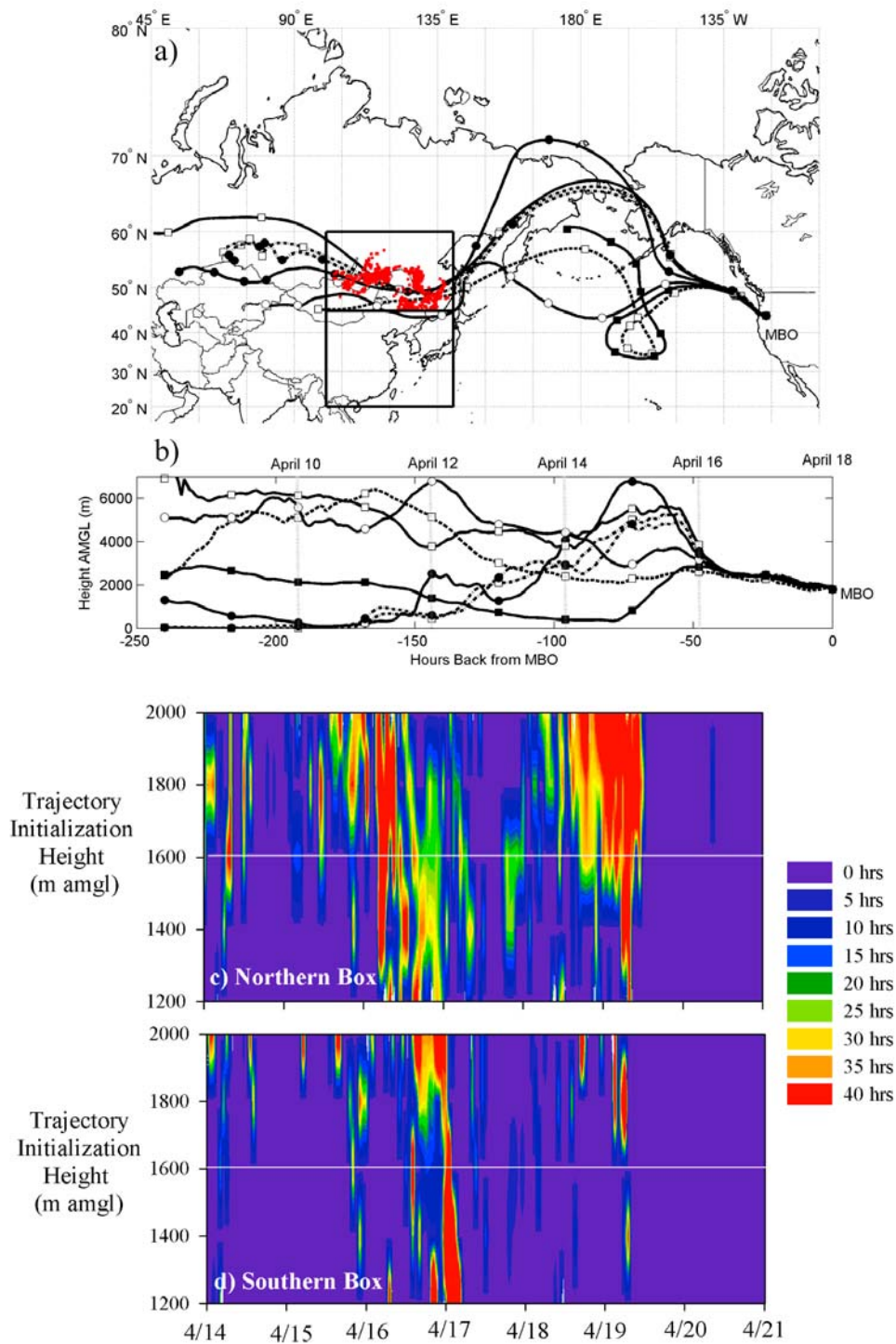


Figure 6. (a) Plain view of representative 10 day HYSPLIT backward trajectories (GDAS grid) initialized from 1800 m amgl each hour from 1200 to 1800 GMT 18 April. MODIS active fires for 12–14 April are shown in red. See text for references. (b) Vertical view of HYSPLIT trajectories. (c) Total residence time of back trajectories in the northern Asian box as a function of time and starting altitude from MBO. (d) Total residence time of back trajectories in the southern Asian box as a function of time and starting altitude from MBO. The white lines in Figures 6c and 6d indicate the approximate height of MBO on the basis of the pressure in the GDAS meteorological grid used by HYSPLIT for the trajectory calculations.

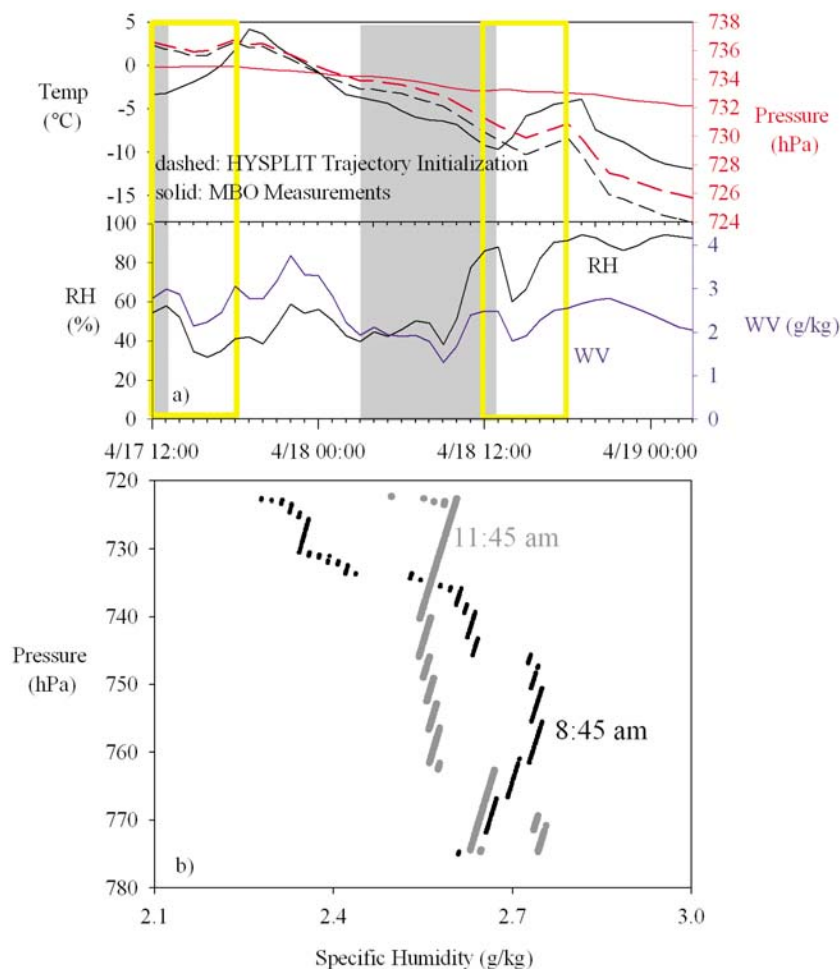


Figure 7. (a) Meteorological parameters at MBO during 17–18 April pollution event. In the top panel, the initialization values of T and pressure for the EDAS 40 km backward HYSPLIT trajectories are also included (dashed). As in Figure 5, the shading indicates approximate sunset to sunrise and time is in GMT. The yellow boxes surround the two FT-influenced morning periods used in the calculations in Table 2. (b) Two specific humidity profiles on the morning of 18 April; times are in PDT.

confirm that the plume was observed free from BL influences during two morning periods, and these two FT-influenced periods are highlighted by the yellow boxes in Figures 5 and 7a.

[36] Figure 8a presents a series of 3-day backward trajectories calculated using the EDAS-40 km grid for the event. There was a slight shift from northerly to northwesterly descent over the plume event. On the basis of the shift in the O_3 to PAN ratio that occurred at 1200 GMT 18 April (see Figure 5a), we divided the event into two parts. The plume was warmer during the first portion of the event when it was observed at MBO, even though the trajectories indicate that the rate of descent was fairly consistent during the 24 h prior to reaching MBO (Figure 8b). Over the 48 h prior to reaching MBO, the portion of the plume observed on 18 April descended from slightly higher altitudes. More importantly, the temperature during the subsidence was different. Figure 8c presents the average temperature along the trajectories over the 48 h prior to reaching MBO. The first portion of the event, characterized by a large O_3 enhancement and a minimal PAN enhancement, traveled to

MBO under warmer conditions than the second part of the event, characterized by a small O_3 enhancement and a larger PAN enhancement.

[37] The trajectory analysis, in conjunction with the in situ soundings, suggests that we observed a plume during two morning periods when MBO was under the influence of the FT. The temperature during subsidence was different for the two portions of the plume, with the later portion arriving at MBO $\sim 5^\circ\text{C}$ colder (Figure 8c and Table 2).

[38] Ozone production efficiency (OPE) is traditionally defined as the O_3 produced per molecule of NO_x oxidized to nitric acid (HNO_3) [Liu *et al.*, 1987]. Understanding the impact of Asian NO_x on O_3 in the western U.S. is a matter of great interest [Hudman *et al.*, 2004; Zhang *et al.*, 2008], and OPE links NO_x emissions to O_3 production. We can estimate the OPE per unit of PAN decomposed using the two morning periods when the plume was observed at MBO. The parameters used in this calculation are given in Table 2. Several assumptions are necessary. First, we assume that plume is well mixed and the same plume type was sampled throughout the event. We cannot confirm this because there

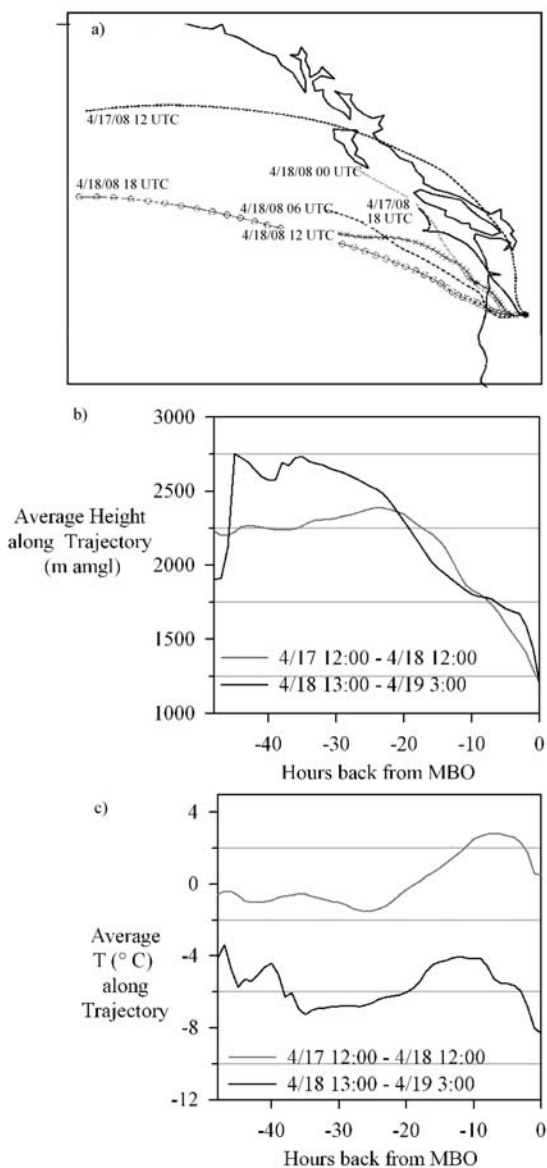


Figure 8. (a) Examples of HYSPLIT backward trajectories run with the EDAS 40 km grid for 17–18 April. The trajectories were initialized from 1200 m above model ground level (amgl) which is the approximate height of MBO on the basis of the pressure in the EDAS grid. The trajectory labels indicate the initialization time from MBO. (b) Average height along backward trajectories initialized from MBO from 17 April 1200 GMT to 18 April 1200 GMT (gray) and from 18 April 1300 GMT to 19 April 0300 GMT (black). (c) Average temperature along backward trajectories initialized from MBO from 17 April 1200 GMT to 18 April 1200 GMT (gray) and from 18 April 1300 GMT to 19 April 0300 GMT (black).

is a period of missing CO data at MBO; however, the HYSPLIT trajectories calculated using the EDAS 40 km grid confirm descending northwesterly flow throughout the period of interest. Therefore, the likelihood that we observed North American pollution is low. Second, we assume that all the NO_x released from the thermal decomposition of PAN has

formed HNO_3 and is therefore no longer contributing to O_3 production. On the basis of our assumption, the calculation presented next may underestimate OPE. The assumption that NO_x is in chemical steady state between the source from PAN decomposition and the loss from oxidation to HNO_3 has been applied previously in a similar context [Hudman *et al.*, 2004] and is applicable to the remote Pacific midtroposphere [Jacob *et al.*, 1996]. This is a more stringent assumption than applied here.

[39] We use the hourly average peak O_3 and peak PAN mixing ratios during each stage of the event. The peak PAN mixing ratios during the warm and cold mornings of the event were 224 and 379 pptv, respectively, which corresponds to a difference in PAN potentially because of thermal decomposition of 155 pptv. The peak O_3 mixing ratios during the warm and cold mornings of the event were 74 and 66 ppbv, respectively, corresponding to an enhancement in O_3 in the warm part of the event, because of production driven by PAN decomposition, of 8 ppbv. From the observations, we calculate an OPE of 51 mol/mol. Alternatively, we could use average parameters for the morning periods for a similar calculation (shown in yellow in Figure 5). This approach yields an OPE of 73 mol/mol; this is the calculation presented in Table 2. The OPE calculation was done in two different ways because there are valid arguments for both. The calculation using the maximum PAN and O_3 in the FT periods is useful because these time periods likely represent the most concentrated portions of the plume. The downside of using only the maximum PAN and O_3 is that the calculation is based on only 2 h of data. The calculation using the mean O_3 and PAN avoids this problem; therefore, both calculations are presented. Regardless of which way the calculation is done, the calculated OPE is much higher than observed in the polluted continental BL [Liang *et al.*, 1998].

[40] It is also possible to estimate PAN decomposition using the temperatures along the HYSPLIT trajectories. The lifetime of PAN is dependent on temperature and the NO_2/NO ratio because of cycling between PAN and the acetyl peroxy radical ($\text{CH}_3\text{CO}_3\cdot$). Reaction of $\text{CH}_3\text{CO}_3\cdot$ with NO_2 does not lead to a net loss of PAN, while reaction with NO or with other species (e.g., HO_2 or RO_2) does. A correction accounting for the cycling between PAN and $\text{CH}_3\text{CO}_3\cdot$ acts to extend the lifetime of PAN [Brasseur *et al.*, 1999; Jacob *et al.*, 1996; Roberts, 2007]. This correction can be large in polluted environments [Roberts, 2007], reducing the rate at which PAN is permanently lost via thermal decomposition by up to 70%. Considering the

Table 2. Comparison of Average Hourly PAN, O_3 , and Temperature for the Periods 17 April 1200–1800 GMT and 18 April 1200–1800 GMT

	17 April 1200–1800 GMT “Warm Plume”	18 April 1200–1800 GMT “Cold Plume”
Hourly average T , °C	−1.4	−6.6
Hourly average PAN, pptv	166	261
Hourly average O_3 , ppbv	66	59
Calculation	PAN decomposed = 261 pptv − 166 pptv = 95 pptv O_3 produced = 66 ppbv − 59 ppbv = 7 ppbv $\text{O}_3/\text{PAN} = 73 \text{ mol/mol}$	

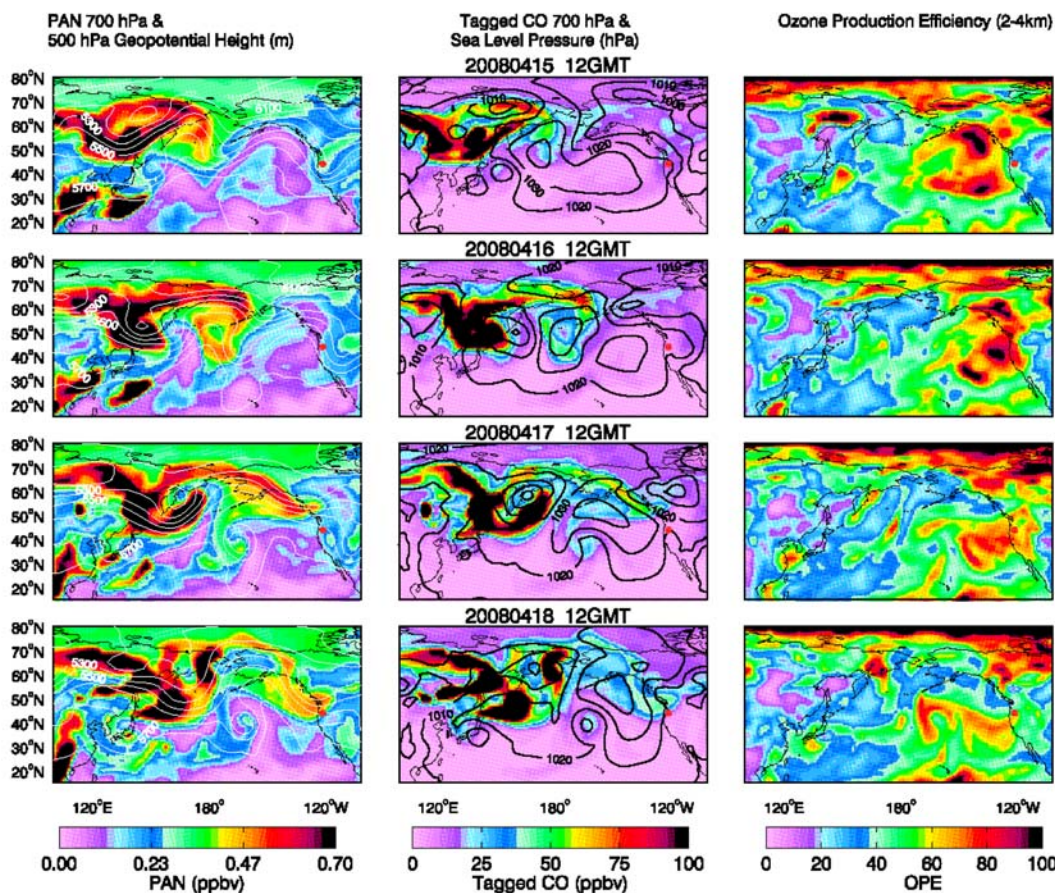


Figure 9. (left) GEOS-Chem simulated PAN mixing ratios at 700 and 500 hPa geopotential height (m) for 15–18 April 2008. (middle) GEOS-Chem simulated tagged Siberian biomass burning CO at 700 hPa and sea level pressure (hPa) for 15–18 April 2008. (right) Mean simulated ozone production efficiency per unit NO_x consumed (OPE) for 15–18 April in the lower free troposphere (FT, average between 2 and 4 km altitude).

relatively low NO_x levels and the low NO_2 -to- NO ratio observed at MBO, we do not expect the correction to be this large in the case presented here. However, it is important to account for cycling between PAN and $\text{CH}_3\text{CO}_3\cdot$ to prevent overestimating PAN loss.

[41] We used the mean temperature along the trajectories associated with the warm portion of the event (17 April 1200 GMT–18 April 1200 GMT) and the peak hourly average PAN (379 pptv) during the cold morning of the event to calculate the potential PAN loss due to thermal decomposition. Following *Brasseur et al.* [1999], we used the average observed NO_2/NO ratio (1.3) for 0900 PDT–1100 PDT on 17 and 18 April at MBO, and calculated an effective lifetime of PAN which accounted for cycling between PAN and $\text{CH}_3\text{CO}_3\cdot$. The average NO_2/NO ratio observed at MBO was used because it is the best estimate of within-plume NO_x mixing ratios available. On the basis of the temperature, decomposition of ~ 197 pptv of PAN was possible in the plume in 48 daylight hours (this calculation is only relevant in the presence of NO), indicating that the trajectory temperatures during subsidence are broadly consistent with our previous estimate of PAN loss. We repeated the same calculation using the mean temperature along the trajectories associated with the cold portion of the event and

the PAN (379 pptv) during the cold morning of the event. This calculation suggests less PAN loss (~ 111 pptv) due to thermal decomposition under the colder conditions.

[42] The NO_2/NO ratio that we observed at MBO and that was used in this calculation was relatively low. It is possible to increase the NO_2/NO ratio by a factor of 2 before the recycling between PAN and $\text{CH}_3\text{CO}_3\cdot$ is sufficient to make this calculation inconsistent with the calculation of OPE. As an additional consistency check, we compared our observationally based estimate of OPE to that obtained from the GEOS-Chem model. The right column of Figure 9 shows model calculated OPE for 2–4 km for April 15–18. The model predicts a region of relatively high OPE (>50 mol/mol) in the Gulf of Alaska on April 15–16, consistent with our observationally based calculations. The middle column of Figure 9 shows GEOS-Chem tagged Siberian biomass burning CO for 1200 GMT April 15–18. GEOS-Chem supports a fire source for the plume observed at MBO 17–18 April. Finally, the left column in Figure 9 shows the GEOS-Chem calculated 700 hPa PAN. The model shows the plume traveling over the great circle, in agreement with the trajectories.

[43] HNO_3 and total reactive nitrogen (NO_y) were not measured at MBO during spring 2008. However, the

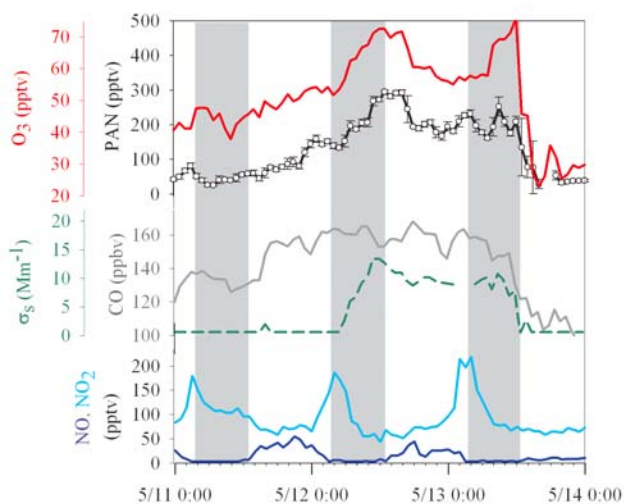


Figure 10. (a) Time series of gas phase species and $1\text{-}\mu\text{m}$ σ_{sp} during the plume observed at MBO on 11–14 May. The shading indicates approximate sunset to sunrise. Time is in GMT. σ_{sp} was below detection limit for the first portion of the period shown.

GEOS-Chem simulated HNO_3 and PAN mixing ratios for MBO over the period 17–18 April are broadly consistent with our implicit assumption that NO_y was conserved during this period. The GEOS-Chem output is considered here because the model captures the magnitude of PAN observed at MBO (~ 400 pptv) and the observed temperature transition during this particular time period (Figure 5b).

[44] *Hudman et al.* [2004] calculated an OPE of 53 mol/mol in the eastern Pacific on the basis of the average PAN and O_3 measured in two different plumes encountered 12 days apart by the NOAA WP-3D aircraft during the 2002 ITCT 2K2 mission [*Nowak et al.*, 2004]. A higher OPE (80 mol/mol) was reported on the basis of GEOS-Chem calculations [*Hudman et al.*, 2004]. Typical OPEs at similar latitudes in the continental BL and the lower FT over North America are on the order of 10 and 20 mol/mol, respectively [*Hudman et al.*, 2004; *Liang et al.*, 1998]. *Hudman et al.* [2004] suggest that the OPE in the Pacific Northwest FT is particularly high because of the combination of strong radiation, low humidity, and low background NO_x concentrations.

[45] NO_x levels at MBO are higher than those observed via aircraft in the remote central or eastern Pacific at similar altitudes [*Bertram*, 2006; *Singh et al.*, 1998], and we suspect this to be largely because of the fact that MBO experiences a greater continental influence given its location. However, in comparison to other continentally influenced high-altitude sites in North America, the values of NO_x observed at MBO are on the lower end of what has been observed [*Murphy et al.*, 2006a, 2006b, 2006c; *Parrish et al.*, 1990]. Most akin to the observations seen at MBO are those from springtime measurements at the alpine research station Jungfraujoch (3580 m) in the Swiss Alps [*Zanis et al.*, 2000; *Zellweger et al.*, 2003].

3.2.2. The 12–13 May Plume

[46] A second Asian pollution plume impacted MBO on 12–13 May, and a time series is presented in Figure 10. CO , O_3 , and PAN mixing ratios rose throughout 11 May,

with a sharp rise in PAN and O_3 observed on 12 May. The event ended abruptly 1200 GMT 13 May. The peak hourly average PAN mixing ratio during this event (295 pptv) was observed near local sunrise when MBO was under the influence of the FT. CO reached 168 ppbv during this event. Unlike the plume observed during April, the relationship between PAN and O_3 at MBO remained consistent.

[47] Figure 11a presents representative 10-day HYSPLIT back trajectories for the plume. The particular trajectories shown are associated with the 5-h period surrounding the peak measured PAN mixing ratio (1100–1800 GMT 12 May). As in Figure 6c, Figure 11b can be interpreted as a summary of all the 10-day back trajectories for the May pollution event. It indicates that MBO was steadily impacted by air that had previously passed over Asia. Similar to the previous event, most of the trajectories that passed through the Asian BL (below 3 km in the box shown), passed through the northeastern portion of the region encompassed by the box in Figure 11a. As fires were also noted in this region during the first 2 weeks of May, this plume could have either an anthropogenic or biomass burning source. This plume took a more southerly route across the Pacific than the plume observed in mid-April. Some of the trajectories initialized at lower elevations at MBO suggest that portions of this air mass descended in the mid-Pacific (as shown in Figure 11a); other trajectories initialized at higher elevations do not show this dip in altitude during transit.

[48] Also shown in Figure 11 is the average height and temperature for the 3-day backward HYSPLIT (EDAS 40-km grid) trajectories initialized from MBO during the event. The plume descended approximately 3000 m during the 48 h prior to reaching MBO. The average temperature along the trajectory was colder than that calculated for either portion of the 17–18 April plume. This plume was also observed at MBO under strongly subsiding conditions, although the synoptic situation differed from the 17–18 April case. Figure 11d shows the rising temperature and pressure (solid lines) observed at MBO throughout the event. As in Figure 7a, the initialization pressure and temperature from the EDAS 40-km trajectories (dashed lines) track the observations, indicating that the trajectories and the underlying meteorological fields captured the regional synoptic situation well. During the air mass descent to MBO, T only reached a maximum of ~ 270 K. The lower panel in Figure 11d shows the RH and WV observed at MBO. The rise in σ_{sp} does not coincide exactly with the rise in the gas phase species (Figure 10) because of local aerosol scavenging due to freezing fog at MBO.

3.3. Synoptic Context of the April and May Asian Plumes

[49] There are limited observations of the effects of PAN decomposition on O_3 production in subsiding pollution plumes in the eastern Pacific FT. Subsidence is generally associated with the springtime climatological high pressure centered near 140°W and 35°N , which creates subsidence over northern California. *Kotchenruther et al.* [2001] observed a subsiding plume during the PHOBEA campaign in spring 1999 under this type of regime. As mentioned in section 3.2.1, several plumes identified during aircraft flights during the ITCT 2K2 campaign have been analyzed by both *Nowak et al.* [2004] and *Hudman et al.* [2004].

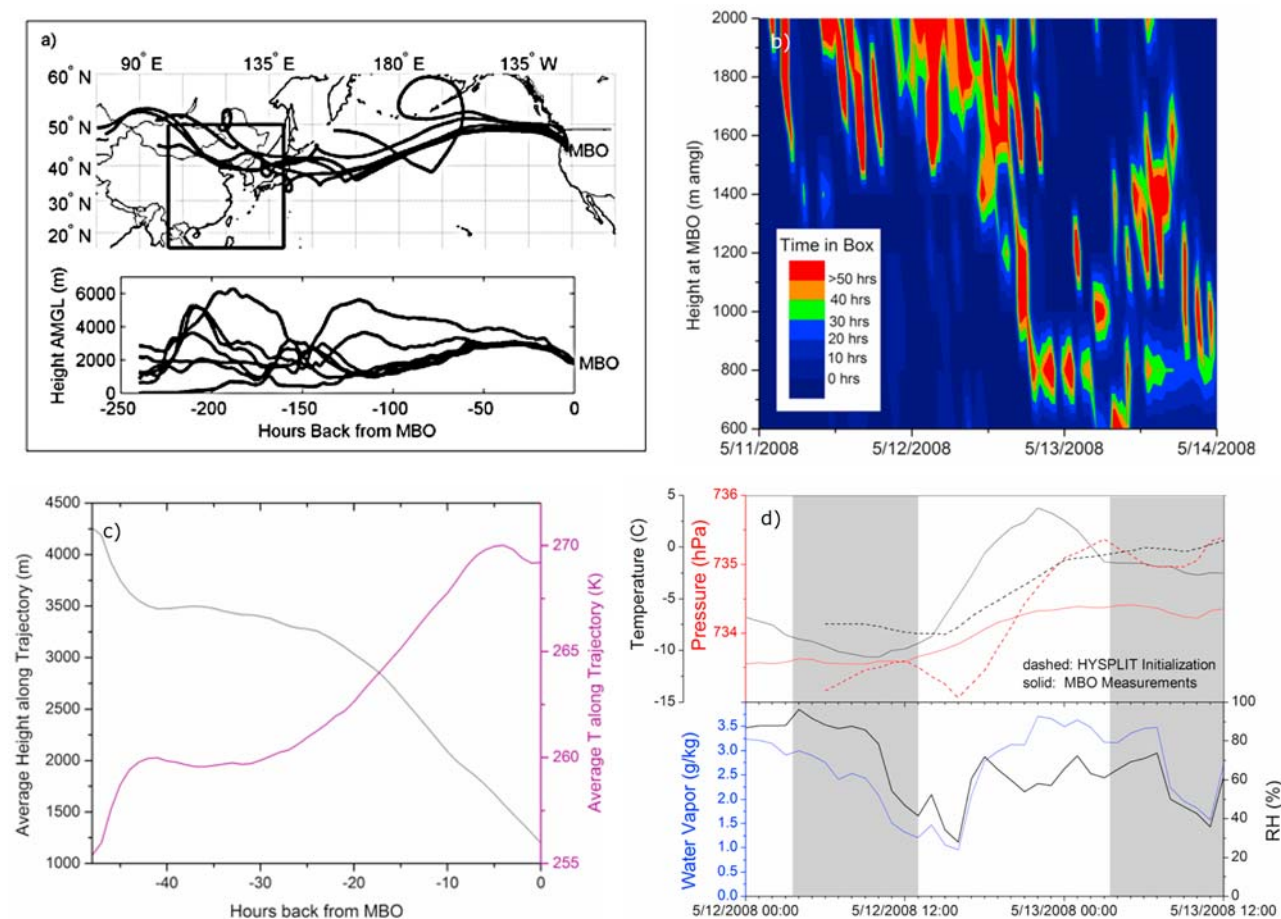


Figure 11. (a) Representative 10-day HYSPLIT backward trajectories initialized from 1400 m amgl each hour from 1100 to 1800 GMT 12 May. These trajectories were initialized during the period with maximum observed PAN mixing ratios. (b) Total residence time of back trajectories in the east Asian box (outlined in gray in Figure 11a) as a function of time and starting altitude from MBO. (c) Average height (black) and temperature (magenta) along HYSPLIT backward trajectories (EDAS 40 km grid) initialized from MBO from 11 May 1200 GMT to 13 May 1200 GMT, and (d) Meteorological parameters at MBO during 12 May pollution event. The shading in Figure 11d indicates approximate sunset to sunrise.

The importance of secondary O_3 production during subsidence in the Pacific high-pressure system was noted by Jaeglé *et al.* [2003]. More recently, Zhang *et al.* [2008] examined the chemical evolution of an Asian pollution plume during trans-Pacific transport that was identified by satellite and aircraft observations during the 2006 INTEX-B campaign. In the same paper, they generalize this case study, in terms of the transport and pattern of O_3 production, to the entire INTEX-B period (mid April–mid May) [Zhang *et al.*, 2008]. They show that as pollution plumes reach the eastern Pacific, the semipermanent springtime Aleutian Low and Pacific High cause the plumes to split into a southern and northern branch. The O_3 production driven by PAN decomposition is expected to be stronger in the southern branch located off the California coast, which is characterized by warm dry subsidence (see Figure 11 by Zhang *et al.* [2008]).

[50] Figure 12 presents the 5 day mean sea level pressure, 700 hPa geopotential height, and 700 hPa vector winds for the April and May events. Despite the common thread of subsidence, the synoptic situations surrounding the

17–18 April and the 12–13 May pollution plumes observed at MBO were notably different. The meteorology supporting the transport of the latter plume was consistent with the framework presented by Zhang *et al.* [2008]; but this was not the case for the 17–18 April plume. The wind speed maximum during this period at 700 hPa was located in the Gulf of Alaska (Figure 12c). The height field indicates strong northwesterly flow from the Gulf of Alaska to the Pacific northwestern U.S. The plume embedded in this flow field arrived at MBO under strong cold air advection, which is apparent in the cloud structure visible in coincident satellite observations (not shown). During April 2008, the Pacific jet stream was stronger and located further north than the climatological mean. Anomalously high surface pressure also extended north to the Aleutian Islands.

[51] The mean synoptic state surrounding the 12–13 May pollution plume was similar to the climatological mean situation for spring in this region (not shown). A prominent Aleutian Low developed and a region of high surface sea level pressure existed off the coast of California (Figure 12d).

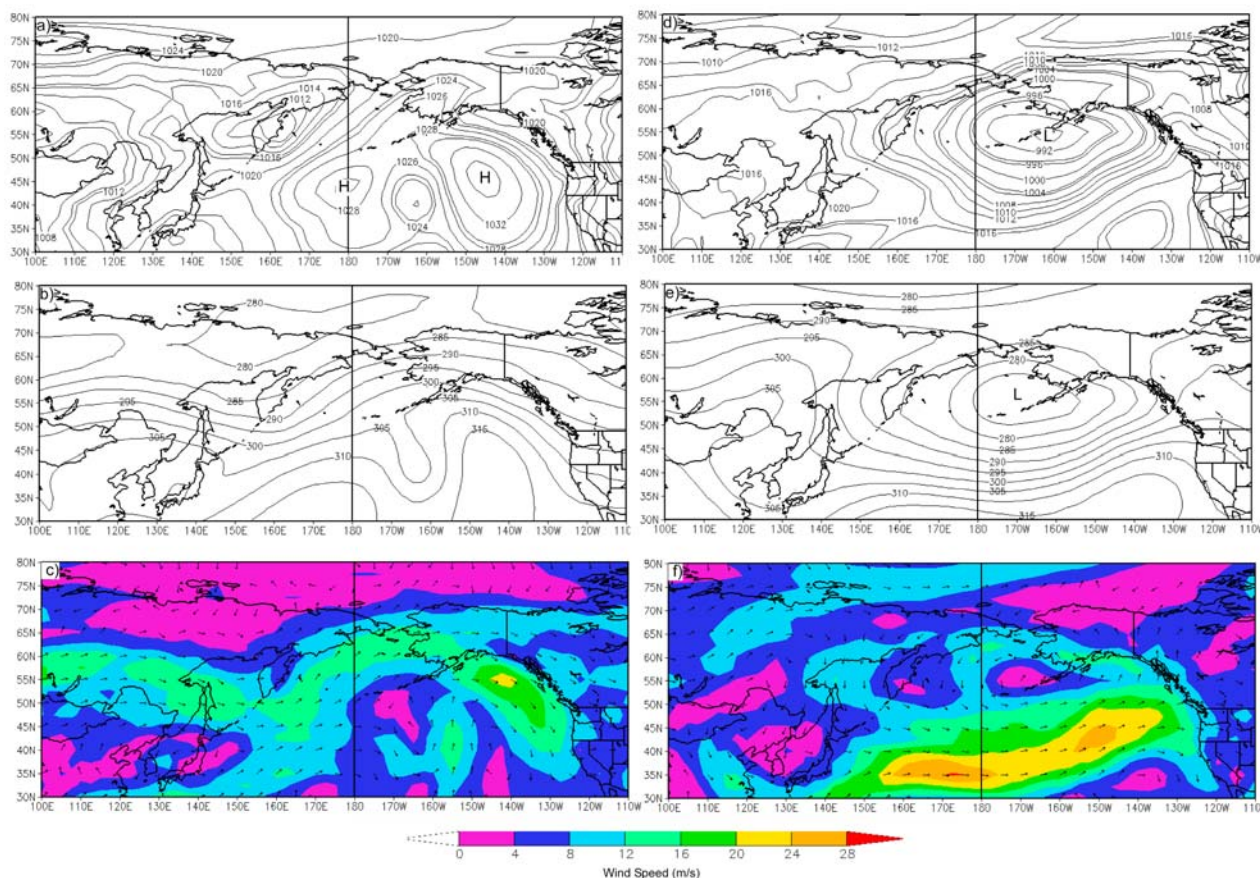


Figure 12. (a) Five day mean sea level pressure field for 15–19 April 2008, (b) 5-day mean 700 hPa geopotential height field for 15–19 April 2008, (c) 5-day mean 700 hPa vector winds for 15–19 April 2008, (d) 5-day mean sea level pressure field for 10–14 May 2008, (e) 5-day mean 700 hPa geopotential height field for 10–14 May 2008, and (f) 5-day mean 700 hPa vector winds for 10–14 May 2008. Images provided by the NOAA/ESRL Physical Sciences Division from <http://www.cdc.noaa.gov/> [Kalnay *et al.*, 1996].

The wind speed maximum at 700 hPa was shifted south, and as indicated by the trajectories in Figure 11a, the plume embedded in this flow field did not travel over the Gulf of Alaska. It took a more southern path, and the type of plume splitting outlined by Zhang *et al.* [2008] was possible during this period. The difference in these two synoptic regimes, both of which resulted in subsiding plumes reaching MBO, illustrates that a stark latitudinal separation of regions of high- and low- O_3 production is not a feature of all descending pollution plumes in the eastern Pacific.

[52] The two different synoptic regimes also created different travel times across the Pacific. The plume observed at MBO on 17–18 April traveled over the great circle, moving from southern Russia to Oregon in ~ 4 days. The 12–13 May plume took a longer more southern path across the Pacific. The plume pathways as simulated by GEOS-Chem were consistent with the HYSPLIT trajectories.

3.4. Relationship Between Trace Gases in the April and May Asian Plumes

[53] PAN was positively correlated with CO in both transport plumes. A reduced major axis (RMA) regression analysis was performed for each plume, and these results are

summarized in Table 3. RMA regression is appropriate when there is error in both the independent and dependent variables [Ayers, 2001]. There was a lower PAN/CO relationship observed during the 17–18 April event compared to the 12–13 May event, which is consistent with the colder subsidence experienced by the 12–13 May plume. However, because the source of the April plume is likely biomass burning in southeastern Russia (<http://firefly.geog.umd.edu/firemap/>), and the NO_x/CO emission ratios for biomass burning and industrial plumes differ, this difference should not solely be interpreted as a result of different subsidence rates or temperatures between the plumes.

Table 3. Regression Statistics for Plume Periods

Time Period (GMT)	PAN/CO Regression Statistics		O_3/CO Regression Statistics	
	RMA Slope, ppbv/ppbv $\times 10^{-3}$	R^2	RMA Slope, ppbv/ppbv $\times 10^{-3}$	R^2
17 April 2100 to 19 April 1200	4.0	0.66	−0.33	0.10
12 May 0000 to 13 May 1500	6.3	0.42	0.73	0.28

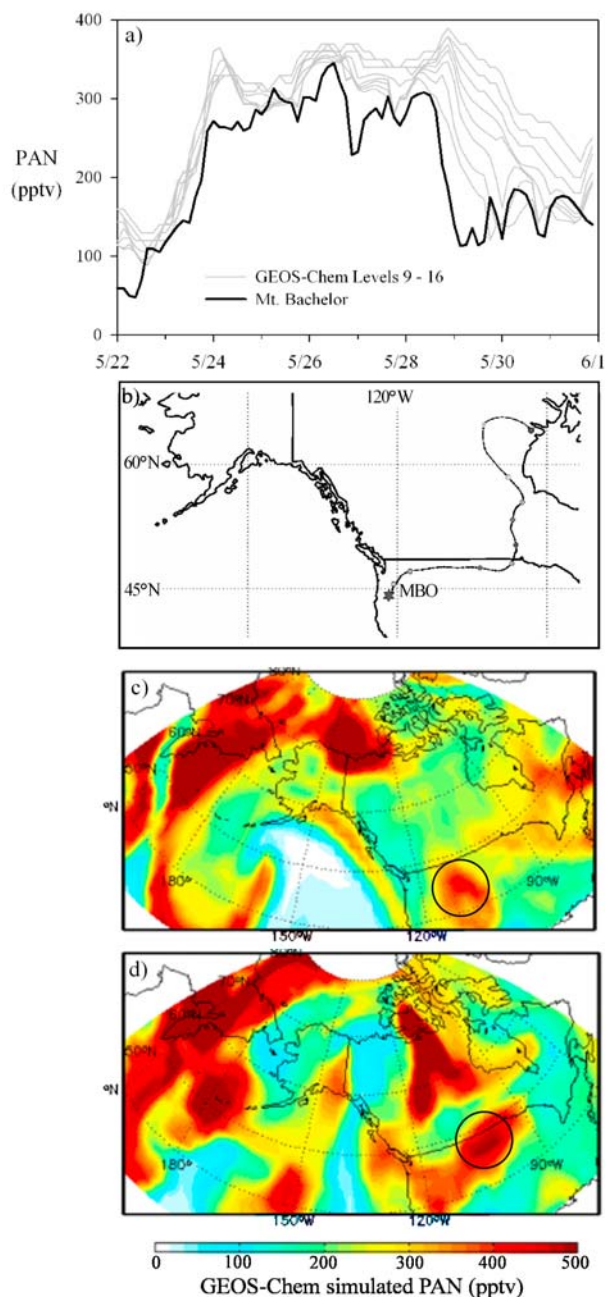


Figure 13. (a) Observed PAN at MBO and GEOS-Chem simulated PAN at MBO for sigma levels 9–16. The levels are roughly equivalent to 874–732 hPa. (b) Ten day HYSPLIT backward trajectory initialized from MBO 0000 GMT 26 May. (c) GEOS-Chem simulated PAN at 700 hPa 0000 GMT 23 April. (d) GEOS-Chem simulated PAN at 700 hPa 1800 GMT 25 April. The circles in Figures 13c and 13d surround the hypothesized source regions for PAN observed at MBO. See text for further information.

[54] A consistent positive relationship was not seen in the O_3 and CO data for these events. Note that CO measurements were not available for the beginning of the 17–18 April plume, and the relationship between O_3 and CO is only presented for the second part of the plume. Over this entire period, O_3 and CO were not significantly correlated. Ozone

was weakly correlated with CO in the 12–13 May plume ($R^2 = 0.28$, $P = 0.004$).

[55] The PAN-CO- O_3 relationships are complicated by transport and chemistry, and it is difficult to account for the relative contributions of these processes. We expect to maintain a linear relationship between these species as a plume is diluted with relatively clean air during transpacific transport, as long as all the dilution air has a consistent PAN-CO- O_3 relationship. This is not the case as the plume chemically ages. Both the thermal decomposition of PAN and O_3 production or destruction are nonlinear processes. The relationships can be further complicated if the plume is mixed with O_3 -rich air of stratospheric origin, or if lightning NO_x emissions are injected into the air mass.

3.5. North American Continental BL PAN Mixing Ratios: 24–29 May

[56] The gray box in Figure 4 surrounds a weeklong period of elevated PAN (median = 290 pptv) observed at MBO during a period of continued North American continental influence. No obvious diurnal variability in PAN mixing ratios was observed during this period (Figure 13a). Periods of elevated CO (~ 160 ppbv) were observed on 25 May, but throughout the remainder of the period of elevated PAN, CO remained < 140 ppbv. Ozone ranged from 38 to 54 ppbv. NO_x data were not available for this period. Fog ($RH > 95\%$) was observed during this period at MBO, with the exception of 26 May 0000 GMT–27 May 1800 GMT, coincident with a period of above detection limit ($1-9 M m^{-1}$) σ_{sp} .

[57] Backward trajectories initialized from MBO on 24, 25, and 26 May show low-level transport out of the Gulf of Alaska, transport shifting from northwesterly to northeasterly, and easterly transport from the North American continental BL, respectively. The trajectories indicate the air arriving at MBO from 26 to 28 May traveled from Hudson Bay, south through the southern Manitoba BL and then west along the Canadian-U.S. border, finally turning south over Washington State to reach central Oregon (Figure 13b). The 700 hPa geopotential height field for 26 May indicates that the easterly flow was the product of two low-pressure regions that developed to the south and east of MBO over California and North Dakota, respectively. Active fires were observed in North Dakota, southern Manitoba, and southeastern Saskatchewan during the week of 20–26 May (<http://firefly.geog.umd.edu/firemap/>).

[58] GEOS-Chem captured the magnitude and timing of the weeklong period of elevated PAN well ($R^2 = 0.78$, GEOS-Chem sigma level 10 versus MBO), so the model was used to identify the origin of the PAN (Figure 13a). The model indicated that the source region for the PAN observed from 23 to 25 May was located in eastern Washington and Idaho (Figure 13c), while the source for the PAN observed from 25 to 29 May was located in the Dakotas, southern Manitoba, and southeastern Saskatchewan (Figure 13d). GEOS-Chem does not support an Arctic contribution to observed PAN at MBO during this period.

[59] This period of PAN observations at MBO is the most appropriate period to compare with previous measurements from the North American BL, and with measurements of PAN from continentally influenced mountain observation sites, such as Jungfraujoch [Lööv *et al.*, 2008; Zellweger *et al.*, 2003; Zellweger *et al.*, 2000]. The PAN mixing ratios

observed at MBO during this continentally influenced period (155–350 pptv) are of a similar magnitude to these previous measurements. Phippen *et al.* [2001] observed median PAN mixing ratios of 231 and 334 pptv during May 1998 and May 1999, respectively, at a rural site in northern Michigan [Phippen *et al.*, 2001]. During 1998–1999, Zellweger *et al.* [2003] observed median PAN mixing ratios of 256 and 334 pptv in undisturbed FT and BL-disturbed FT periods, respectively. Using a different method to identify period of undisturbed FT air, Lööv *et al.* [2008] estimated lower mixing ratios for spring 2005 (mean $\pm 1\sigma = 137 \pm 54.1$ pptv). The mean PAN mixing ratio reported by Lööv *et al.* [2008] associated with undisturbed FT air during spring 2005 is much closer in magnitude to that observed at MBO during 2008 than that reported by Zellweger *et al.* [2003] for two spring seasons in the late 1990s.

4. Conclusions

[60] We have presented an analysis of spring 2008 PAN measurements from the MBO. The range of variability observed in the diurnal cycle was an order of magnitude smaller than the range of PAN measurements, suggesting that PAN mixing ratios at MBO are controlled by synoptic scale processes. Two plumes of Asian origin associated with elevated PAN mixing ratios were identified on the basis of elevated CO, σ_{sp} and back trajectory analysis. These plumes and the associated meteorological conditions were examined in detail. We also highlighted a period when MBO was influenced by North American continental BL air, which was characterized by consistent elevated PAN mixing ratios (median = 290 pptv).

[61] The relationship between PAN and O₃ varied in the 17–18 April Asian plume. We observed a higher PAN-to-O₃ ratio under colder temperatures and a lower PAN-to-O₃ ratio in warmer temperatures, consistent with the production of O₃ from PAN decomposition during warm subsidence. Using in situ vertical profiles of basic meteorological parameters, we were able to segregate two periods of measurements free from BL influences. We used these two periods to derive an O₃ production efficiency (OPE) per unit of NO_x released during PAN decomposition of 51–73 mol/mol. On the basis of this calculation, a substantial amount (~8 ppbv) of the observed ~20 ppbv O₃ enhancement can be attributed to recent PAN decomposition. The 17–18 April plume provides an example of the hemispheric impact biomass burning can have on the composition of the remote FT.

[62] The second Asian long-range transport event (observed during May) was more dilute, characterized by lower CO mixing ratios and σ_{sp} than the April event. There was more PAN relative to the amount of CO measured, consistent with the colder subsidence temperatures calculated by backward trajectories. Both events occurred under subsiding conditions, and trajectories indicate descent to MBO over the 48 h prior to the air masses reaching MBO. We show that the synoptic situation was different during the two major Asian events observed during this spring campaign. The April event was characterized by strong subsidence associated with pronounced cold air advection. The subsidence during the May event occurred under strengthening high pressure. The case studies presented here illustrate that PAN decomposition

to produce NO_x and subsequently O₃ depends critically on the local temperature regime. We also show that a stark latitudinal separation between regions of high and low O₃ production may not be a feature of all descending pollution plumes in the eastern Pacific.

[63] It is evident from this analysis that plumes of O₃ precursors are imported into the North American FT. Assessing the integrated importance of these plumes for North American air quality requires further research in two key areas. First, we need a better understanding of how these plumes are diluted and chemically processed as they are mixed down from the FT into the BL. Second, we need a multiyear consistent observational record of O₃ precursors to determine the frequency of these events and the inter-annual variability in the PAN import flux.

[64] **Acknowledgments.** Emily V. Fischer was supported by a Department of Energy Graduate Research Environmental Fellowship. Support for the Mount Bachelor Observatory was provided by the National Science Foundation under Grant ATM-0724327. We would like to thank Frank Flocke for loaning us the ECD used in the custom gas chromatograph. We also gratefully acknowledge the support provided by the Mount Bachelor maintenance staff.

References

- Ayers, G. P. (2001), Comment on regression analysis of air quality data, *Atmos. Environ.*, 35, 2423–2425, doi:10.1016/S1352-2310(00)00527-6.
- Bertram, T. H. (2006), Observational constraints for the source strengths, transport and partitioning of reactive nitrogen on regional and global scales, Ph.D. thesis, Dep. of Chem., Univ. of Calif., Berkeley.
- Bey, I., D. J. Jacob, J. A. Logan, and R. M. Yantosca (2001a), Asian chemical outflow to the Pacific in spring: Origins, pathways, and budgets, *J. Geophys. Res.*, 106(D19), 23,097–23,113.
- Bey, I., D. J. Jacob, R. M. Yantosca, J. A. Logan, B. D. Field, A. M. Fiore, Q. Li, H. Y. Liu, L. J. Mickley, and M. G. Schultz (2001b), Global modeling of tropospheric chemistry with assimilated meteorology: Model description and evaluation, *J. Geophys. Res.*, 106(D19), 23,073–23,095.
- Brasseur, G. P., J. J. Orlando, and G. S. Tyndall (1999), *Atmospheric Chemistry and Global Change*, 654 pp., Oxford Univ. Press, New York.
- Davies, D. K., S. Iiavajhala, M. M. Wong, and C. O. Justice (2009), Fire information of resource management system: Archiving and distributing MODIS active fire data, *IEEE Trans. Geosci. Remote Sens.*, 47(1), 72–79, doi:10.1109/TGRS.2008.2002076.
- Derwent, R. G., P. G. Simmonds, S. Seuring, and C. Dimmer (1998), Observation and interpretation of the seasonal cycles in the surface concentrations of ozone and carbon monoxide at Mace Head, Ireland from 1990 to 1994, *Atmos. Environ.*, 32(2), 145–157, doi:10.1016/S1352-2310(97)00338-5.
- Draxler, R. R., and G. D. Hess (1998), An overview of the HYSPLIT₄ modelling system for trajectories, dispersion, and deposition, *Aust. Meteorol. Mag.*, 47, 295–308.
- Draxler, R. R., and G. D. Rolph (2003), HYSPLIT (HYbrid Single-Particle Lagrangian Integrated Trajectory), NOAA Air Resour. Lab., Silver Spring, Md. (Available at <http://www.arl.noaa.gov/ready/hysplit4.html>)
- Flocke, F., A. J. Weinheimer, A. L. Swanson, J. M. Roberts, R. Schmitt, and S. Shertz (2005), On the measurement of PANs by gas chromatography and electron capture detection, *J. Atmos. Chem.*, 52, 19–43, doi:10.1007/s10874-005-6772-0.
- Giglio, L., and J. Descloitres (2003), An enhanced contextual fire detection algorithm for MODIS, *Remote Sens. Environ.*, 87(2–3), 273–282, doi:10.1016/S0034-4257(03)00184-6.
- Guenther, A., T. Karl, P. Harley, C. Wiedinmyer, P. I. Palmer, and C. Geron (2006), Estimates of global terrestrial isoprene emissions using MEGAN (Model of Emissions of Gases and Aerosols from Nature), *Atmos. Chem. Phys.*, 6, 3181–3210.
- Heald, C. L., et al. (2003), Asian outflow and trans-Pacific transport of carbon monoxide and ozone pollution: An integrated satellite, aircraft, and model perspective, *J. Geophys. Res.*, 108(D24), 4804, doi:10.1029/2003JD003507.
- Holloway, T., H. Levy II, and P. Kasibhatla (2000), Global distribution of carbon monoxide, *J. Geophys. Res.*, 105(D10), 12,123–12,147.
- Hudman, R. C., et al. (2004), Ozone production in transpacific Asian pollution plumes and implications for ozone air quality in California, *J. Geophys. Res.*, 109, D23S10, doi:10.1029/2004JD004974.

- Jacob, D. J., et al. (1996), Origin of ozone and NO_x in the tropical troposphere: A photochemical analysis of aircraft observations over the South Atlantic basin, *J. Geophys. Res.*, *101*(D19), 24,235–224,250.
- Jaeglé, L., D. A. Jaffe, H. U. Price, P. Weiss-Penzias, P. I. Palmer, M. J. Evans, D. J. Jacob, and I. Bey (2003), Sources and budgets for CO and O₃ in the northeastern Pacific during the spring of 2001: Results from the PHOBEA-II Experiment, *J. Geophys. Res.*, *108*(D20), 8802, doi:10.1029/2002JD003121.
- Jaffe, D., E. Prestbo, P. Swartzendruber, P. Weiss-Penzias, S. Kato, A. Takami, S. Hatakeyama, and Y. Kajii (2005), Export of atmospheric mercury from Asia, *Atmos. Environ.*, *39*, 3029–3038, doi:10.1016/j.atmosenv.2005.01.030.
- Justice, C. O., L. Biglio, S. Korontzi, J. Owens, J. T. Morissette, D. Roy, Roy, J. S. Desdoitres, S. Alleume, F. Petitcolin, and Y. Kaufman (2002), The MODIS fire products, *Remote Sens. Environ.*, *83*, 244–262, doi:10.1016/S0034-4257(02)00076-7.
- Kalnay, E., et al. (1996), The NCEP/NCAR 40-Year Reanalysis Project, *Bull. Am. Meteorol. Soc.*, *77*, 437–471, doi:10.1175/1520-0477(1996)077<0437:TNYRP>2.0.CO;2.
- Kato, N., and H. Akimoto (1992), Anthropogenic emission of SO₂ and NO_x in Asia: Emission inventories, *Atmos. Environ.*, *26A*, 2997–3017.
- Koike, M., et al. (2003), Export of anthropogenic reactive nitrogen and sulfur compounds from East Asia region in spring, *J. Geophys. Res.*, *108*(D20), 8789, doi:10.1029/2002JD003284.
- Kotchenruther, R. A., D. A. Jaffe, and L. Jaegle (2001), Ozone photochemistry and the role of peroxyacetyl nitrate in the springtime northeastern Pacific troposphere: Results from the Photochemical Ozone Budget of the Eastern North Pacific (PHOBEA) campaign, *J. Geophys. Res.*, *106*, 28,731–728,741.
- Kuhns, H., E. M. Knipping, and J. M. Vukovich (2005), Development of a United States–Mexico emissions inventory for the big Bend Regional Aerosol and Visibility Observational (BRAVO) Study, *J. Air Waste Manage. Assoc.*, *55*, 677–692.
- Liang, J., L. W. Horowitz, D. J. Jacob, Y. Wang, A. M. Fiore, J. A. Logan, G. M. Gardner, and J. W. Munger (1998), Seasonal variations of reactive nitrogen species and ozone over the United States and export fluxes to the global atmosphere, *J. Geophys. Res.*, *103*, 13,435–413,450.
- Liu, H., D. J. Jacob, I. Bey, R. M. Yantosca, B. N. Duncan, and G. W. Sachse (2003), Transport pathways for Asian pollution outflow over the Pacific: Interannual and seasonal variations, *J. Geophys. Res.*, *108*(D20), 8786, doi:10.1029/2002JD003102.
- Liu, S. C., M. Trainer, F. C. Fehsenfeld, D. D. Parrish, E. J. Williams, D. W. Fahey, G. Hubler, and P. C. Murphy (1987), Ozone production in the rural troposphere and the implications for regional and global ozone distributions, *J. Geophys. Res.*, *92*(D4), 4191–4207, doi:10.1029/JD092iD04p04191.
- Logan, J. (1985), Tropospheric ozone: Seasonal behavior, trends, and anthropogenic influence, *J. Geophys. Res.*, *90*(D6), 10,463–410,482.
- Lööv, B. J. M., S. Henne, G. Legreid, J. Staehelin, S. Reimann, A. S. H. Prévôt, M. Steinbacher, and M. K. Vollmer (2008), Estimation of background concentrations of trace gases at the Swiss Alpine site Jungfraujoch (3580 m asl), *J. Geophys. Res.*, *113*, D22305, doi:10.1029/2007JD009751.
- Moxim, W. J., H. Levy II, and P. S. Kasibhatla (1996), Simulated global tropospheric PAN: Its transport and impact on NO_x, *J. Geophys. Res.*, *101*(D7), 12,621–612,638.
- Murphy, J. G., D. A. Day, P. A. Cleary, P. J. Wooldridge, and R. C. Cohen (2006a), Observations of the diurnal and seasonal trends in nitrogen oxides in the western Sierra Nevada, *Atmos. Chem. Phys.*, *6*, 5321–5338.
- Murphy, J. G., D. A. Day, P. A. Cleary, P. J. Wooldridge, D. B. Millet, A. H. Goldstein, and R. C. Cohen (2006b), The weekend effect within and downwind of Sacramento: Part 2. Observation evidence for chemical and dynamical contributions, *Atmos. Chem. Phys.*, *6*, 11,971–12,019.
- Murphy, J. G., D. A. Day, P. A. Cleary, P. J. Wooldridge, D. B. Millet, A. H. Goldstein, and R. C. Cohen (2006c), The weekend effect within and downwind of Sacramento: Part 1. Observations of ozone, nitrogen oxides, and VOC reactivity, *Atmos. Chem. Phys.*, *7*, 5327–5339.
- Nowak, J. B., et al. (2004), Gas-phase chemical characteristics of Asian emission plumes observed during ITCT 2K2 over the eastern North Pacific Ocean, *J. Geophys. Res.*, *109*, D23S19, doi:10.1029/2003JD004488.
- Ohara, T., H. Akimoto, J. Kurokawa, N. Horii, K. Yamaji, X. Yan, and T. Hayasaka (2007), An Asian emission inventory of anthropogenic emission sources for the period 1980–2020, *Atmos. Chem. Phys.*, *7*, 4419–4444.
- Olivier, J. G. J., J. P. J. Bloos, J. J. M. Berdowski, A. J. H. Visschedijk, and A. F. Bouwman (1999), A 1990 global emission inventory of anthropogenic sources of carbon monoxide on 1° × 1° developed in the framework of EDGAR/GEIA, *Chemosphere Global Change Sci.*, *1*, 1–17, doi:10.1016/S1465-9972(99)00019-7.
- Parrish, D. D., et al. (1990), Systematic variations in the concentration of NO_x (NO Plus NO₂) at Niwot Ridge, Colorado, *J. Geophys. Res.*, *95*(2), 1817–1836, doi:10.1029/JD095iD02p01817.
- Pippen, M. R., S. B. Bertman, T. Thornberry, M. A. Carroll, and S. Sillman (2001), Seasonal variations of PAN, PPN, and O₃ at the upper Midwest PROPHET site, *J. Geophys. Res.*, *106*(D20), 24,451–424,463.
- Reid, J. S., E. M. Prins, D. L. Westphal, C. C. Schmidt, K. A. Richardson, S. A. Christopher, T. F. Eck, E. A. Reid, C. A. Curtis, and J. P. Hoffman (2004), Real-time monitoring of South American smoke particle emissions and transport using a coupled remote sensing/box-model approach, *Geophys. Res. Lett.*, *31*, L06107, doi:10.1029/2003GL018845.
- Richter, A., J. P. Burrows, H. Nüß, C. Granier, and U. Niemeier (2005), Increase in tropospheric nitrogen dioxide over China observed from space, *Nature*, *437*, 129–132, doi:10.1038/nature04092.
- Roberts, J. M. (2007), PAN and related compounds, in *Volatile Organic Compounds in the Atmosphere*, edited by R. Koppmann, pp. 221–268, Blackwell, Oxford, U. K.
- Roberts, J. M., et al. (2004), Measurement of peroxyacetic nitric anhydrides (PANs) during the ITCT 2K2 aircraft intensive experiment, *J. Geophys. Res.*, *109*, D23S21, doi:10.1029/2004JD004960.
- Singh, H. B., and L. J. Salas (1986), Global distribution of peroxyacetyl nitrate, *Nature*, *321*, 588–591, doi:10.1038/321588a0.
- Singh, H. B., et al. (1998), Latitudinal distribution of reactive nitrogen in the free troposphere over the Pacific Ocean in late winter/early spring, *J. Geophys. Res.*, *103*(D21), 28,237–228,246.
- Stohl, A. (1998), Computation, accuracy, and applications of trajectories—A review and bibliography, *Atmos. Environ.*, *32*, 947–966, doi:10.1016/S1352-2310(97)00457-3.
- Streets, D. G., Q. Zhang, L. Wang, K. He, J. Hao, Y. Wu, Y. Tang, and G. R. Carmichael (2006), Revisiting China's CO emissions after the transport and chemical evolution over the Pacific (TRACE-P) mission: Synthesis of inventories, atmospheric modeling, and observations, *J. Geophys. Res.*, *111*, D14306, doi:10.1029/2006JD007118.
- Talukdar, R. K., J. B. Burkholder, A.-M. Schmolter, J. M. Roberts, R. Wilson, and A. R. Ravishankara (1995), An investigation of the loss processes for peroxyacetyl nitrate in the atmosphere: UV photolysis and reaction with OH, *J. Geophys. Res.*, *100*, 14,163–114,173.
- Trentmann, J., and M. O. Andreae (2003), Chemical process in a young biomass-burning plume, *J. Geophys. Res.*, *108*(D22), 4705, doi:10.1029/2003JD003732.
- van Aardeene, J. A., G. R. Carmichael, H. I. Levy, D. Streets, and L. Hordijk (1999), Anthropogenic NO_x emissions in Asia in the period 1990–2020, *Atmos. Environ.*, *33*, 633–646, doi:10.1016/S1352-2310(98)00110-1.
- Vestreng, V., and H. Klein (2002), Emission data reported to UNECE/EMEP: Quality assurance and trend analysis and presentation of WebDab, report, Norw. Meteorol. Inst., Oslo.
- Volz-Thomas, A., I. Xueref, and R. Schmitt (2002), An automatic gas chromatograph and calibration system for ambient measurements of PAN and PPN, *Environ. Sci. Pollut. Res.*, *4*, 72–76.
- Warneke, P., and T. Zerbach (1992), Synthesis of peroxyacetyl nitrate by acetone photolysis, *Environ. Sci. Technol.*, *26*(1), 74–79, doi:10.1021/es00025a005.
- Weiss-Penzias, P., D. Jaffe, P. Swartzendruber, J. B. Dennison, D. Chand, W. Hafner, and E. Prestbo (2006), Observations of Asian air pollution in the free troposphere at Mount Bachelor Observatory during spring of 2004, *J. Geophys. Res.*, *111*, D10304, doi:10.1029/2005JD006522.
- Weiss-Penzias, P., D. Jaffe, P. Swartzendruber, W. Hafner, D. Chand, and E. Prestbo (2007), Quantifying atmospheric mercury emissions from biomass burning and East Asian industrial regions based on ratios with carbon monoxide in pollution plumes at the Mount Bachelor Observatory, *Atmos. Environ.*, *41*(21), 4366–4379, doi:10.1016/j.atmosenv.2007.01.058.
- Wolfe, G. M., J. A. Thornton, V. F. McNeill, D. A. Jaffe, D. Zeidmiller, D. Chand, J. Smith, P. Swartzendruber, F. Flocke, and W. Zheng (2007), Influence of trans-Pacific pollution transport on acyl peroxy nitrate abundances and speciation at Mount Bachelor Observatory during INTEX-B, *Atmos. Chem. Phys.*, *7*(20), 5309–5325.
- Yienger, J. J., M. Galanter, T. A. Holloway, M. J. Phadnis, S. K. Guttikunda, G. R. Carmichael, W. J. Moxim, and H. Levy II (2000), The episodic nature of air pollution transport from Asia to North America, *J. Geophys. Res.*, *105*(D22), 26,931–26,945.
- Zanis, P., P. S. Monks, E. Schuepbach, L. J. Carpenter, T. J. Green, G. P. M. Iils, S. Bauguitte, and S. A. Penkett (2000), In situ ozone production under free tropospheric conditions during FRETEX '98 in the Swiss Alps, *J. Geophys. Res.*, *105*(D19), 24,223–24,234, doi:10.1029/2000JD900229.
- Zellweger, C., M. Ammann, B. Buchmann, P. Hofer, M. Lugauer, R. Ruttimann, N. Streit, E. Weingartner, and U. Baltensperger (2000), Summer-time NO_y speciation at the Jungfraujoch, 3580 m asl, Switzerland, *J. Geophys. Res.*, *105*, 6655–6667.

Zellweger, C., J. Forrer, P. Hofer, S. Nyeki, B. Schwarzenbach, E. Wellingarter, M. Ammann, and U. Baltensperger (2003), Partitioning of reactive nitrogen (NO_y) and dependence on meteorological conditions in the lower free troposphere, *Atmos. Chem. Phys.*, *3*, 779–796.

Zhang, Q., et al. (2007), NO_x emission trends for China, 1995–2004: The view from the ground and the view from space, *J. Geophys. Res.*, *112*, D22306, doi:10.1029/2007JD008684.

Zhang, L., et al. (2008), Transpacific transport of ozone pollution and the effect of recent Asian emission increases on air quality in North America:

An integrated analysis using satellite, aircraft, ozonesonde, and surface observations, *Atmos. Chem. Phys. Discuss.*, *8*, 8143–8191.

E. V. Fischer, L. Jaeglé, and D. R. Reidmiller, Department of Atmospheric Sciences, University of Washington, 408 ATG Bldg., Box 351640, Seattle, WA 98195, USA. (efischer@atmos.washington.edu)

D. A. Jaffe, Science and Technology Program, University of Washington-Bothell, Bothell, WA 98011, USA.